Mosher, D.C., Erbacher, J., and Malone, M.J. (Eds.)
Proceedings of the Ocean Drilling Program, Scientific Results Volume 207

2. Sediment Composition and Cyclicity in the Mid-Cretaceous at Demerara Rise, ODP Leg 207[1]

Alexandra J. Nederbragt,[2] Jürgen Thurow,[2] and Richard Pearce[3]

ABSTRACT

Mid-Cretaceous organic-rich sediments of mainly Cenomanian and Turonian age were recovered during Ocean Drilling Program (ODP) Leg 207 along a presumed paleowater depth transect on Demerara Rise. The entire sequence shows decimeter- to meter-scale cyclic alternations between carbonate-rich and organic-rich sediments. An interpretation of the cyclic pattern is derived from time series analysis of sediment color data in selected intervals in combination with thin section analysis of representative lithologies. Results are compared to time-equivalent sediments in the Tarfaya Basin, Morocco.

At Demerara Rise, there are two main types of carbonate-rich lithologies: pelagic carbonate beds and planktonic foraminiferal packstone layers. Pelagic carbonate-rich intervals are present throughout the two deepwater sites (ODP Sites 1257 and 1258) and in the upper part of the sequence at the shallower sites (Sites 1259–1261). Planktonic foraminiferal packstones are attributed to either current- or wave-induced winnowing in relatively shallow water. Packstones are the dominant carbonate-rich lithology in the lower part of the sequence at Sites 1259–1261 but decrease in frequency higher in the sequence because of continued subsidence; they persist longer at the two shallowest sites (Sites 1259 and 1261) than at the intermediate water depth site (Site 1260). Cyclic variation in lithology at Demerara Rise is inferred to represent eccentricity and precession cycles with, at most, a weak obliquity component. Large variations in the thickness of the inferred precession cycles are attributed to climate-dependent variation in sedimentation rates of carbonate and siliciclastic material in combination with vari-

[1]Nederbragt, A.J., Thurow, J., and Pearce, R., 2007. Sediment composition and cyclicity in the mid-Cretaceous at Demerara Rise, ODP Leg 207. *In* Mosher, D.C., Erbacher, J., and Malone, M.J. (Eds.), *Proc. ODP, Sci. Results,* 207: College Station, TX (Ocean Drilling Program), 1–31. doi:10.2973/odp.proc.sr.207.103.2007
[2]Department of Earth Sciences, University College London, Gower Street, London WC1E 6BT, UK. Correspondence author: **a.nederbragt@ucl.ac.uk**
[3]School of Ocean and Earth Science, University of Southampton, National Oceanography Centre, Southampton, European Way, Southampton SO14 3ZH, UK.

Initial receipt: 23 August 2005
Acceptance: 14 February 2007
Web publication: 24 April 2007
Ms 207SR-103

able degrees of compaction and, within packstone layers, variable rates of removal of sediment because of winnowing. Lithologic cycles within the latest Cenomanian oceanic anoxic event are correlative between the Tarfaya Basin and Demerara Rise.

A weak obliquity signal at Demerara Rise, in contrast to the strong obliquity component inferred for the Tarfaya Basin, can be explained if the obliquity signal represents variation in subsurface ventilation. The sequence at Demerara Rise represents continuous anoxia, suggesting that any variation in ventilation would have little impact if all oxygen is consumed before it could reach the area. The strong eccentricity–precession bundles are inferred to represent an atmospheric and/or oceanic circulation signal, which controlled rainfall and siliciclastic sedimentation rates as well as upwelling intensity and surface water productivity. Winnowing of carbonate-rich layers at shallow water depths at Demerara Rise implies that general circulation, and thus any upwelling, was most vigorous during deposition of carbonate-rich levels, which ultimately implies that organic-rich sediments are primarily related to enhanced anoxia.

INTRODUCTION

A major step in paleoclimate research during the past 40 years has been the recognition of orbital cycles, or Milankovitch cycles, as the pacemaker for large-scale climate fluctuations during the Quaternary (Shackleton and Opdyke, 1973; Imbrie, 1985). However, the present climate is controlled overall by an icehouse situation, where fluctuations in the global ice volume dominate climatic trends on orbital timescales. This situation is unusual with respect to much of the Phanerozoic. For long periods, significant ice shields did not exist. Climate, especially during the Paleogene and Mesozoic, is thought to have been equable, yet the characteristic patterns of Milankovitch cycles can still be recognized in rhythmically bedded sediments. Such cycles are meanwhile used widely to determine rates of sediment accumulation, providing an estimate for the duration of major climate events like the late Paleocene Thermal Maximum (e.g., Norris and Röhl, 1999) or mid-Cretaceous oceanic anoxic events (OAEs) (e.g., Kuhnt et al., 1997; Erbacher et al., 2001; Wilson and Norris, 2001). However, the climate forcing mechanisms that produce the observed lithologic variations in the absence of significant ice shields are poorly understood.

With the problems caused by modern global warming, interest in extreme climatic conditions in the geologic past has revived, as the extreme climatic conditions provide a natural laboratory to test the sensitivity of the Earth system to large climate perturbations. One of the targets is the climate during the mid-Cretaceous (90–120 Ma), which led to widespread deposition of organic-rich sediments. Schlanger and Jenkyns (1976) first recognized that increased rates of organic carbon burial occurred preferentially during certain time intervals, or OAEs. However, fundamental questions about the cause of OAEs remain unsolved. In particular, it is still debated whether high carbon burial rates are the result of increased productivity or of better preservation under anoxic conditions (Stein, 1986; Arthur et al., 1987; Calvert, 1987; Erbacher et al., 2001; Nederbragt et al., 2001; Wilson and Norris, 2001; Kuypers et al., 2002). One of the main obstacles was (is) the lack of chemically well-preserved deepwater sections on land and incomplete recovery at marine drill sites.

During Ocean Drilling Program (ODP) Leg 207 (Demerara Rise, western equatorial North Atlantic) (Fig. F1), a thick sequence of mid-Cretaceous organic-rich sediments of predominantly Cenomanian and Turonian age (89–99 Ma) was recovered at five sites along a paleowater depth transect (Fig. F1) (Erbacher, Mosher, Malone, et al., 2004). The material offers a unique opportunity to obtain a much more detailed and accurate reconstruction of oceanic change under a range of different greenhouse climate conditions. The entire sequence shows decimeter- to meter-scale (Milankovitch scale) cyclic alternations between light-colored, carbonate-rich and dark-colored, organic carbon-rich sediments (Erbacher, Mosher, Malone, et al., 2004). The sequence is representative for background greenhouse conditions in the equatorial North Atlantic region (cf. Kuhnt et al., 1990; Erlich et al., 1999). The sequence at Demerara Rise includes OAE2, the latest Cenomanian event that was one of the most severe OAEs of the entire mid-Cretaceous. Here we present a sedimentological and cyclostratigraphic analysis of the organic-rich unit to determine which sedimentary processes shaped the lithological cycles, with the ultimate aim to unravel the underlying climate processes that operate on orbital timescales under extreme greenhouse conditions. We also correlate the Leg 207 sites with the similar sediment sequence in the Tarfaya Basin farther east along the northwest African coast (Fig. F1), to explore how the depositional environment varied along the tropical North Atlantic margin.

F1. Paleogeographic reconstruction at 100 Ma, p. 21.

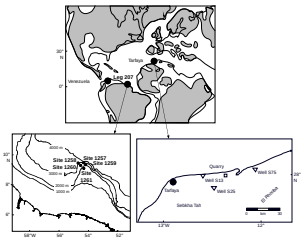

GEOLOGICAL SETTING

The mid-Cretaceous organic-rich unit was recovered at all five sites that were drilled during Leg 207 (Erbacher, Mosher, Malone, et al., 2004). The unit is as thick as ~80-m, and total organic carbon (TOC) content is frequently >10 wt%, with maximum values >25 wt%, especially within OAE2 (Erbacher et al., 2005). The Leg 207 sites represent a presumed mid-Cretaceous depth transect from deep depths at Sites 1258 and 1257 to shallower depths at Sites 1259–1261. The occurrence of laminated sediments throughout the unit indicates a depth of deposition below permanent wave base, which corresponds to depth of >50–70 m in the modern open ocean. There is no sign in the precruise seismic profiles that the sites were in a semirestricted basin. However, because of the virtual absence of benthic foraminifers it is not possible to refine the paleowater depth any further.

The mid-Cretaceous sediments at Demerara Rise are representative of the wider equatorial North Atlantic margin (Fig. F1). To the east, northwest Africa was a conjugate margin, as the connection with the South Atlantic was still closed or, at most, open for surface water circulation only. The sediment sequence in the Tarfaya Basin (Morocco) (Fig. F1) has been studied from both outcrops and industrial drill holes (Kuhnt et al., 1990, 2005). The La Luna Formation in Venezuela forms the continuation to the west of Demerara Rise (Erlich et al., 1999). In all three regions, shallow-water sediments were deposited during the Albian, followed by rapid drowning of the shelf toward the end of the Albian. The Cenomanian and younger sediment sequences are (hemi)pelagic, organic-rich, and show cyclic variation in carbonate and organic carbon content. The region was the center for burial of organic matter (OM) in the circum-North Atlantic, culminating during OAE2 (Kuhnt et al., 1990). The main phase of OM burial ended during the Coniacian–Santonian when the connection with the South Atlantic opened fully.

Biostratigraphic control within the mid-Cretaceous unit at Demerara Rise is poor because of the scarcity of age-diagnostic nannofossils and planktonic foraminifers (Erbacher, Mosher, Malone, et al., 2004). Even though calcareous microfossils are generally abundant, the assemblages consist almost exclusively of long-ranging opportunistic species. Very low diversity planktonic foraminiferal faunas similar to those at Demerara Rise are also found in the mid-Cretaceous throughout Venezuela (Erlich et al., 1999). The scarcity of biostratigraphic marker species points to some form of "extreme" and/or highly variable surface water conditions throughout the wider region. Age-diagnostic species, both among nannofossils and planktonic foraminifers, are usually most abundant under oligotrophic open-ocean conditions (Roth and Krumbach, 1986; Nederbragt, 1999). Very low diversity assemblages occur under a range of conditions, including hyper- and hyposaline conditions and very shallow water. However, the most likely reason for low-diversity assemblages at Demerara Rise are high surface water productivity or, in the case of planktonic foraminifers, a very shallow oxygen minimum zone impinging on the depth habitat of subsurface dwelling species. The main effect in practice is that only large-scale biostratigraphic units could be recognized within the mid-Cretaceous at Demerara Rise (Erbacher, Mosher, Malone, et al., 2004). However, further age control in the interval around OAE2 is provided by the stable carbon isotope stratigraphy of Erbacher et al. (2005), which shows that deposition of the organic-rich unit is diachronous (Fig. F2).

F2. Schematic distribution of major lithologies at Sites 1258–1261 and in Well S13, p. 22.

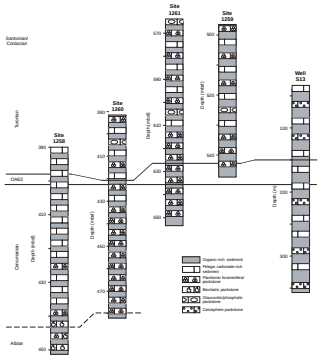

MATERIAL AND METHODS

Color records for ODP Sites 1257–1261 were generated for individual cores from shipboard Geoscan II digital images following published methods (Schaaf and Thurow, 1994; Nederbragt and Thurow, 2004). The shipboard photospectrometer reflectance data show substantial random scatter in laminated sediments. Because of the small spot size (typically 1 mm) and the relatively wide sample spacing (2.5 cm), distinct millimeter-scale color fluctuations between dark and light laminae are not sampled adequately. The continuous time series that were extracted from the Geoscan II images have the advantage that color values can be integrated over a wider interval to produce statistically more representative average values. The red, green, and blue channels in the image were translated into L*a*b* coordinates, in which L* represents lightness and a* and b* represent the hue of the sediment (Erbacher, Mosher, Malone, et al., 2004; Nederbragt and Thurow, 2004). In this paper we use b*, which represents yellow (positive values) and blue (negative values).

Analysis of sediment texture is based on slab samples from representative lithologies at Sites 1257–1261 in combination with shipboard thin sections from discrete samples. Polished thin sections were made of a selection of the slab samples using techniques described in Pike and Kemp (1996) and analyzed with a scanning electron microscope (SEM) used in backscattered electron (BSE) mode. Additional samples were split along light laminae and prepared for standard secondary electron SEM analysis to determine the composition of fecal pellets. The Geoscan II images were logged to determine the stratigraphic distribution of different lithologies.

Grayscale records have been compiled in the Tarfaya Basin for industrial Well S75 (Fig. F1) (Kuhnt et al., 1997) and a set of slab samples

from a nearby quarry (Ravilious, 2002). Thin sections studied for this paper are mainly from the quarry, in which sediments representing the upper part of OAE2 are exposed, in combination with a limited number of samples from the lower Cenomanian to upper Turonian in Well S13 (Thurow et al., 1988). Color records from Leg 207 and the Tarfaya Basin are cross-correlated to each other using tie points provided by published stable carbon isotope stratigraphies (Erbacher et al., 2005; Kuhnt et al., 2005). Blackman-Tukey power spectra are calculated with the time series analysis package Analyseries (Paillard et al., 1996). Bandpass and low-pass filtering of the color time series was performed in the frequency domain (Press et al., 1992) to extract the cyclic pattern in specific frequency bands.

LITHOLOGY AND SEDIMENT TEXTURE

Figure F2 shows a summary of the mid-Cretaceous stratigraphy at Demerara Rise compared to the Tarfaya Basin. The sequence in both areas consists of a cyclic alternation between dark, organic-rich and light, carbonate-rich intervals. The sediment fabric of the organic-rich intervals is essentially the same in all sections in both areas throughout the Cenomanian–Turonian. The composition of the carbonate-rich levels is more variable, both within and between sections. Representative examples of the different lithologies are illustrated in Plates P1, P2, and P3. The main lithologic difference between Demerara Rise and the Tarfaya Basin is in clay content. Quartz sand/silt is present in the lower part of the Cenomanian sequence in the Tarfaya Basin, but clay is virtually absent. Carbonate content is generally between 50 and 90 wt%, and TOC content ranges up to 15 wt%. The remainder of the sediment is thought to consist of finely dispersed silica (Kuhnt et al., 1997). In contrast, clay is present in variable quantities throughout the Cenomanian–Turonian at Demerara Rise. With the exception of carbonate concretions, carbonate content is usually ~50 wt% or less in organic-rich layers (Erbacher, Mosher, Malone, et al., 2004).

Organic-Rich Intervals

Dark sediments are invariably laminated in both areas. Thin sections show a stacking of fecal pellets and lenses of organic matter, with or without dispersed small planktonic foraminifers (Pl. P1, fig. 7; Pl. P3, figs. 1–3). The number of planktonic foraminifers often varies considerably from one lamina to the next. The faunas are dominated by small species (*Heterohelix moremani* and *Hedbergella delrioensis;* triserial *Guembelitria* is present). Large specimens are rare; when present, they usually are concentrated in a single lamina (Pl. P3, fig. 8). Nannofossils are commonly concentrated in fecal pellets (Pl. P1, fig. 4; Pl. P3, figs. 3, 4). Sediments in the Tarfaya Basin contain frequent large fecal pellets, which often consist of near-monospecific nannofossil assemblages. Pellets with near-monospecific *Eprolithus floralis* floras are especially easy to recognize in BSE images (Pl. P3, figs. 3, 4). Such large fecal pellets are rare at Sites 1259–1261 at Demerara Rise and very rare at Sites 1257 and 1258. Organic-rich levels at the Leg 207 sites frequently contain abundant phosphate stringers and nodules, whereas such features are rare in the Tarfaya samples.

P1. TLM and SEM photographs, p. 29.

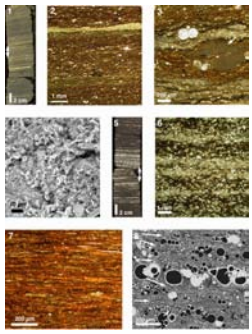

P2. TLM photographs, p. 30.

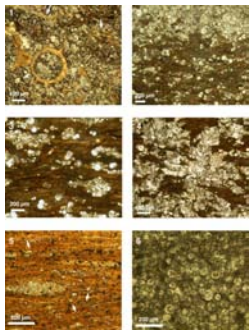

P3. Samples from the OAE2 interval in the Tarfaya Basin quarry, p. 31.

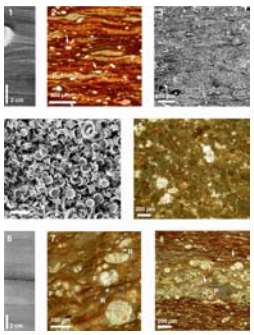

Carbonate-Rich Intervals

Carbonate-rich layers are composed usually of the same basic components as organic-rich layers, but they are present in different proportions relative to each other. The two dominant carbonate-rich lithologies are pelagic carbonate-rich beds and packstones. Carbonate-rich beds at Demerara Rise are usually laminated. In the Tarfaya Basin, they are often bioturbated before and after OAE2 and usually faintly laminated within OAE2. In addition, part of the carbonate-rich layers, especially at Demerara Rise, are recrystalized or micritized to the extent that the original sediment fabric is no longer visible.

Pelagic Carbonates

Pelagic carbonate-rich intervals consist predominantly of fecal pellets with fewer and smaller organic-rich lenses than in the surrounding organic-rich layers. Planktonic foraminifers are more variable in size. The faunas are still dominated by small specimens/species, but larger specimens (>250 µm; *Whiteinella* spp. and *Heterohelix globulosa*) are common (Pl. **P1,** figs. 2, 3; Pl. **P3,** fig. 7). Planktonic foraminifers are more abundant in some laminae than in others, but they are generally dispersed within the sediment as individual specimens. Only very rarely are they clustered in fecal pellets (Pl. **P2,** fig. 3).

Pelagic carbonates are the dominant carbonate-rich lithology throughout Sites 1257 and 1258 (except for the lowest part of the Cenomanian), and within OAE2 in the Tarfaya Basin (Fig. **F2**). They are present at Site 1260 within OAE2 and in the Turonian and at Sites 1259 and 1261 in the upper part of the Turonian and in younger sediments (Fig. **F1**). Pelagic carbonates at Demerara Rise are faintly to distinctly laminated, often with white micritic laminae that probably consisted of coccolith-rich fecal pellets originally, whereas dark laminae reflect relatively high clay content (Pl. **P1,** figs. 1–3). Carbonate-rich layers within OAE2 in the Tarfaya Basin are generally faintly laminated to homogeneous (Pl. **P3,** figs. 6, 7).

Packstones

Carbonate-rich packstones at Demerara Rise commonly form distinctly laminated decimeter-scale intervals that typically consist of alternating light planktonic foraminiferal packstones and darker wackestones (Pl. **P1,** figs. 5, 6; Pl. **P2,** fig. 2). The transition between the wackestone and packstone laminae is gradual given the scale of the laminae (Pl. **P2,** fig. 2). Laminations are usually parallel and continuous across the width of the core surface, but in some intervals they show indications of very low angle cross-stratification (Erbacher, Mosher, Malone, et al., 2004). The planktonic foraminifers in the packstone laminae are larger than those in the pelagic sediments. The small specimens that are so abundant in the pelagic intervals seem to be especially underrepresented in the packstones. Planktonic foraminiferal packstones are the dominant carbonate-rich lithology in the lower part of the sequence at Sites 1259–1261, but they become less prominent higher in the sequence at all three sites (Fig. **F2**). They are essentially absent at Sites 1257 and 1258, except for an isolated 1-cm-thick packstone with a sharp base, which is probably turbiditic in origin (Pl. **P2,** fig. 1).

Other types of packstones at Demerara Rise form a minor part of the lithology. They consist of coarse bioclastic packstones in the lower part

of the organic-rich sequence at Sites 1257 and 1258 and glauconitic/phosphatic packstones at Sites 1259–1261 in the upper part of the sequence. Bioclastic packstones have planktonic foraminifers as well as the occasional benthic foraminifer in the matrix, and part of the beds are graded. They are interpreted as turbidites or tempestites. The glauconitic/phosphatic packstones are confined to a relatively thin interval within the Turonian at Sites 1259–1261. Age dating is not good enough to determine if deposition was synchronous at all three sites.

In the Tarfaya Basin, part of the carbonate-rich beds both before and after OAE2 consist of calcisphere packstones similar to a rare example from Demerara Rise shown in Plate **P2,** figure 6. The frequency of calcisphere beds in the Tarfaya Basin could not be determined from the limited amount of sample material that is available from Well S13.

Diagenetic Carbonate

Secondary carbonate is present as micrite, sparite filling the tests of foraminifers and any further pore space, and coarsely crystalline sparite replacing the original sediment. Part of the pelagic carbonates at Demerara Rise and most of the carbonate-rich beds in the Tarfaya Basin are micritized to some extent. Fecal pellets in such beds are less compressed than in organic-rich beds (cf. e.g., Pl. **P3,** figs. 3, 7), indicating that the micrite represents an early diagenetic feature. Foraminifers in carbonate-rich levels in both regions are virtually always filled with sparitic cement. Pore space between foraminifers in the packstones at Demerara Rise is also frequently filled with sparite (Pl. **P2,** fig. 2). Coarse crystalline calcite was found only at Demerara Rise. Isolated crystals are pinnacle shaped, growing perpendicular to the bedding plane; any sediment left between crystals is deformed but essentially unaltered (Pl. **P2,** fig. 4). Erbacher, Mosher, Malone, et al. (2004) suggested that this type of sparite could be related to disassociation of gas hydrates, but $\delta^{13}C$ measurements to test this hypothesis are not yet available.

In most cases, secondary calcite probably enhances a preexisting contrast between carbonate-rich and carbonate-poor lithologies. However, the presence of diagenetic carbonate is not always indicative of high primary (pelagic) carbonate content. The example in Plate **P2,** figure 4, shows sparite pinnacles replacing a dark lithology with small fecal pellets and medium-sized planktonic foraminifers, which probably had a relatively low carbonate content originally. Furthermore, the exposure in the quarry in the Tarfaya Basin, where lateral variation in lithology can be traced more easily, shows that limestone nodules are also present within organic-rich beds. Laminae in the surrounding sediment curve around the nodule (Pl. **P3,** fig. 1), whereas fecal pellets within the nodule are not compacted (Pl. **P3,** fig. 5), showing that the nodule is a very early diagenetic feature. Similar nodular limestones are much more difficult to recognize consistently in the narrow-diameter drill cores at Demerara Rise. Curved or tilted laminae are found above or below several of the indurated limestone levels in the Leg 207 cores, suggesting that nodular limestones may be relatively common.

Other Features

BSE imagery of an organic-rich interval from Site 1259 shows occasional examples of lamina couplets that may represent an annual signal. Planktonic foraminifers of variable size are aligned in individual lamina, which are separated by thin, clay-rich laminae (Pl. **P1,** fig. 8). Such fea-

tures never continue for more than a few couplets, and the laminae are not continuous laterally. The thickness of the couplets depends on the size of the foraminifers but is typically on the order of 100 µm.

A feature that is essentially impossible to reconstruct is the primary distribution of radiolarians. Calcified radiolarians are present in the carbonate-rich beds in the Tarfaya Basin (Pl. **P3,** fig. 7), but their presence appears to represent preservational bias rather than their primary abundance pattern. They are most common in the transition to the surrounding organic-rich beds. They are rare in the center of the carbonate-rich levels and absent in the organic-rich levels. Preserved radiolarians are very rare at Demerara Rise (Erbacher, Mosher, Malone, et al., 2004), but some organic-rich levels contain abundant zeolites (clinoptilolite) (Pl. **P2,** fig. 5), which commonly form as a diagenetic product in association with dissolution of radiolarians (Thurow, 1988).

CYCLOSTRATIGRAPHY

Power spectra are calculated against depth for selected cores with full recovery. As input time series we use b* (yellow or blue) rather than the more commonly used L*. Very high values are found for L* (light) in some levels with concretionary limestones, whereas values throughout the remainder of the core are substantially lower (Erbacher, Mosher, Malone, et al., 2004). In contrast, the b* data show much more gradual fluctuations. Pelagic carbonates usually show a strong positive correlation between L* and b* if carbonate content exceeds ~10 wt% (Nederbragt and Thurow, 2004) (i.e., pure chalk is yellowish white). The sharp and abrupt peaks in L* in the Leg 207 cores, which are not accompanied by an increase in b*, could well reflect the presence of very bright but colorless diagenetic calcite and/or cement. Whatever their origin, such discrete peaks dominate power spectra for L* time series to the extent that the presence of other cycles is obscured. We therefore use b* time series because they give results that are easier to interpret.

Most power spectra yielded split peaks (Figs. **F3, F4, F5, F6, F7**) because of variable sedimentation rates and/or degree of compaction. Our aim was to generate an interpretation of the cycle pattern to determine which orbital cycles are actually present and how their thickness varies within the section. To this purpose, power spectra were run against stratigraphic thickness to identify the dominant periodicities. Bandpass and low-pass filters were then applied to the b* time series to isolate those cycles for visual inspection and to explore where in the section those cycles are present and how their amplitudes vary. The expected characteristic patterns are a bundling of ~5 precession cycles into one eccentricity cycle and a relatively constant amplitude for the obliquity cycle (Berger, 1978). Duration of the precession and obliquity cycles was shorter in the past. Interpolation of estimates of Berger et al. (1989) suggest values during the mid-Cretaceous of ~20 k.y. (18.5 and 22.3 k.y.) for the precession cycle and ~38.8 k.y. for the obliquity cycle.

After interpretation of the cycle pattern, we measured the thickness of each inferred precession cycle and calculated the average b* value in the corresponding interval as an indicator for carbonate content (Figs. **F3, F4, F5, F6, F7**). The examples shown are for an interval with predominantly pelagic carbonate-rich beds (Core 207-1259B-22R, Turonian; Fig. **F3**), two intervals with planktonic foraminiferal packstones (Core 207-1259B-23B, Turonian, in Fig. **F4,** and Core 207-1260B-37R,

F3. Cycle pattern in Core 207-1259B-22R, p. 23.

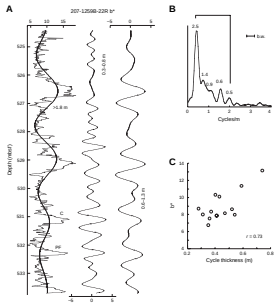

F4. Cycle pattern in Core 207-1259B-23R, p. 24.

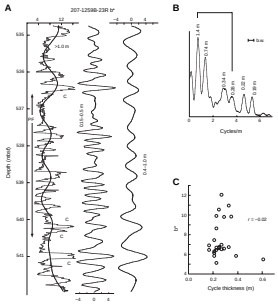

F5. Cycle pattern in Core 207-1260B-37R, p. 25.

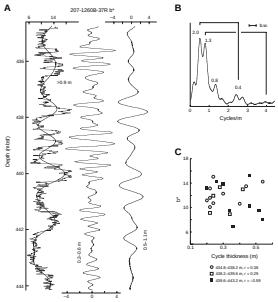

F6. Cycle pattern in Core 207-1260B-35R, p. 26.

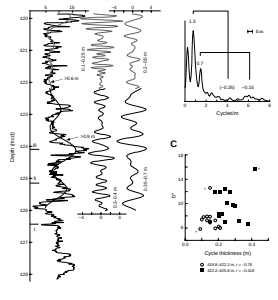

Cenomanian, in Fig. F5) and the OAE2 interval (Core 207-1260B-35R in Fig. F6 and Core 207-1258A-42R in Fig. F7).

Core 207-1259B-22R contains only pelagic carbonate-rich levels, with the exception of one foraminiferal sand at 532.2 meters below seafloor (mbsf) (Fig. F3) (Erbacher, Mosher, Malone, et al., 2004). The power spectrum for b* shows a pronounced peak at 2.5 m, which traces the broad peaks in pelagic carbonate levels but excludes the foraminiferal sand at 532.5 mbsf (Fig. F3). Slightly enhanced power at wavelengths of 0.64 and 0.50 m are interpreted as precession cycles with variable thickness. The bandpass filter in a broad band around the corresponding frequencies shows the expected increase and decrease in amplitude. However, the main feature is a pronounced change in thickness, from broad carbonate-rich peaks to much thinner cycles in intervals with lower b* values (Fig. F3C). The shoulder in the power spectrum at a wavelength of 0.9 m is in the appropriate position for an obliquity cycle. A bandpass filter around this frequency captures mainly the thick carbonate-rich levels in the core, this time including the foraminiferal packstone. However, the filtered data show stronger variation in amplitude than would be expected for an obliquity cycle (Fig. F3A).

Core 207-1259B-23R contains mainly planktonic foraminiferal packstones surrounded by pelagic and diagenetic carbonate levels in the top and bottom parts of the core (Fig. F4). The power spectrum shows a single eccentricity peak with a wavelength of 1.4 m, but power in the precession range is distributed over a wide range of frequencies corresponding to wavelengths between 0.19 and 0.34 m. The peak in the spectrum at 0.74 m is shifted slightly relative to expected wavelength for the obliquity cycle (0.4×1.4 m = 0.56 m), but the bandpass filter around this wavelength suggests that there is indeed an obliquity component. The obliquity bandpass filter, especially in the middle part of the core, tends to group one thin and one thick carbonate-rich cycle (Fig. F4A). Overall, there is high variability in cycle thickness but there is no correlation with b* intensity. The correlation coefficient for all beds with b* is $r = -0.02$; excluding specific beds or specific lithologies does not change the coefficient significantly.

Core 207-1260B-37R shows a combination of thick (~75 cm) and thin (15–40 cm) foraminiferal packstones. The resulting power spectrum shows a split peak representing the long cycle in b*, which is interpreted as the eccentricity cycle, with enhanced power at wavelengths of 2.0 and 1.3 m (Fig. F5). A low-pass filter shows that the 1.3-m cycle is located in the middle of the core between ~438.2 and 439.6 mbsf, while the 2.0-m cycle is present both below and above this interval. The 1.3-m cycle also traces the one clear instance in Core 207-1260B-37R of a typical eccentricity–precession bundle (i.e., a group of five short cycles with increasing–decreasing amplitude). However, a bandpass filter around the expected wavelength of the precession cycle (2.0 m/5 and 1.3 m/5, or 40–25 cm) indicates that such waxing/waning in amplitude is present throughout the core. On the other hand, the color pattern below 439.6 mbsf shows two 2.0-m cycles both consisting of one broad carbonate interval and one broad dark interval, a pattern that is not typical for an eccentricity cycle. However, the precession bandpass filter shows that those broad peaks both contain three short cycles overprinted on the long-term trend. We therefore interpret the broad carbonate-rich peaks as an amalgamation of three precession cycles. However, the consequence of this interpretation is that carbonate sedimentation rates in the broad peak (~80 cm for three precession cycles) must have been lower than in the intervening organic-rich interval

F7. Cycle pattern in Core 207-1258A-42R, p. 27.

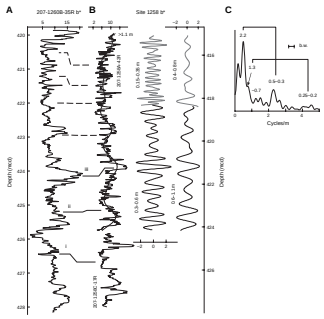

(~120 cm for two precession cycles) (Fig. F5C). Additionally, the power spectrum shows a peak at 0.8 m, which has the right wavelength for an obliquity cycle relative to the 2.0-m eccentricity cycle. Yet the corresponding bandpass filter shows more fluctuation in amplitude than expected for an obliquity cycle, similar to results in Figure F3.

Published $\delta^{13}C$ records across OAE2 provide chronostratigraphic tie points to correlate color records, not only between different sites on Demerara Rise (Erbacher et al., 2005) but also between Leg 207 and the Tarfaya Basin, for which published grayscale records are available (Kuhnt et al., 2005). Color records for Sites 1258 and 1260 show a very similar cycle pattern, although sedimentation rates are different (Figs. F6, F7). Power spectra were calculated for Cores 207-1258A-42R and 207-1260B-35R; Core 207-1258C-17R, which contains the lower part of the excursion at Site 1258 (Fig. F7), was not included because of uncertainties in the exact depth scale because of a coring gap. The corresponding interval in Core 207-1260B-35R was also excluded because of lack of well-defined color cycles in the lower part of OAE2 (Fig. F6). Both power spectra show a split eccentricity cycle due to a sudden change in cycle thickness (sedimentation rates) toward the top of the core. In Core 207-1260B-35R the average precession cycle thickness below and above the change in sedimentation rate is 25 cm and 15 cm, respectively. Core 207-1260B-35R also shows a strong 400-k.y. eccentricity cycle, which traces two maximum amplitude 100-k.y. cycles within and after the $\delta^{13}C$ excursion. Core 207-1260B-35R also shows much more reduced power in the expected precession frequency range. However, the precession bandpass filter for both cores trace a similar pattern with changes in amplitude that are consistent with the inferred eccentricity cycle. Visually, all precession-scale color cycles can be traced between Cores 207-1260B-35R and 207-1258A-42R with the provision that many of those cycles have a double peak in Core 207-1258A-42R (Fig. F7; inspection of the core photographs suggests that the double peaks may be related to increased concentrations of phosphate stringers and nodules near the transition between carbonate-rich and carbonate-poor lithologies). As in the examples in Figures F3 and F5, there is indication in the power spectra for Core 207-1258A-42R of (slightly) enhanced power in the obliquity frequency range (Fig. F7C), but again the bandpass shows a more variable amplitude than expected.

Visual comparison of Demerara Rise with the Tarfaya Basin suggests that the carbonate-rich–organic-rich cycle pattern is broadly comparable at both localities. The color records for Site 1258 and Well S75 in the Tarfaya Basin are especially in phase within the resolution of the $\delta^{13}C$ stratigraphies (Fig. F8). The two basins show a very similar pattern of fluctuation within the $\delta^{13}C$ excursion. The onset of the excursion occurs in an organic-rich interval in both sections; maximum $\delta^{13}C$ values are reached near the top of a carbonate-rich bed. That this bed has very high amplitude in b* at Site 1258 is because of recrystallization. The $\delta^{13}C$ plateau in both sections is characterized by a carbonate minimum followed by a broad carbonate maximum with triple peaks. The correlation above the excursion is more tentative. The noticeable difference between the two sites in this part of the sequence is the presence of a strong long-term cycle (eccentricity) at Site 1258, which is not present in Well S75.

F8. Correlation of $\delta^{13}C$ stratigraphy and sediment color at Site 1258 and Well S75, p. 28.

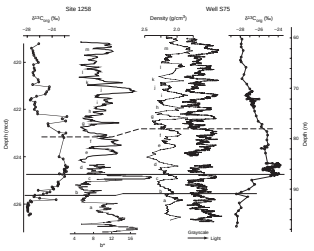

DISCUSSION

One of the aims for this paper was to reconstruct the climate and sedimentation processes that led to the common occurrence of planktonic foraminiferal packstones in large parts of the mid-Cretaceous at Demerara Rise. The two most likely processes to generate such coarse-grained deposits are winnowing or redeposition in gravity deposits or tempestites, which have different implications for the interpretation of the paleoenvironment during the mid-Cretaceous at Demerara Rise. Specifically, the geochemical signature of planktonic foraminifers would not reflect local conditions if a substantial fraction of the material is allochtonous. The fact that packstones appear to occur as a regular part of organic-rich and carbonate-rich cycles implies that they are formed by predictable climate processes. Therefore, to understand their distribution it is necessary to understand the cyclic pattern. However, the spacing of the carbonate-rich and organic-rich cycles appears irregular, with thicknesses varying from meter- to decimeter-scale within single cores. The starting hypothesis for this paper is that the lithological cycles do reflect variation in climate and sediment supply, which was induced by orbital cycles, the only known regular forcing mechanism at the relevant timescales. Still, any underlying regularity could have been modified by random processes or diagenetic alteration to the extent that the orbital cycles are obscured. As a practical application, recognition of Milankovitch cycles in the mid-Cretaceous unit at Demerara Rise would provide information to improve the chronostratigraphic framework. However, the aim here is not to establish a continuous cyclostratigraphy for the entire organic-rich unit but to analyze the cycle pattern in relation to the various lithologies encountered within the mid-Cretaceous. To this purpose, we selected a limited number of individual cores with good recovery from representative lithologies. The relatively irregular nature of the cycles means that standard spectral analysis was not sufficient to illustrate the presence of orbital frequencies.

Very few rhythmically bedded geological sections yield clear-cut power spectra when calculated against stratigraphic depth, whatever the age of the section. Spectral peaks are usually shifted relative to frequencies expected for orbital cycles because of variable sedimentation rates and other nonlinearities. Interpretation of the cycle pattern in the mid-Cretaceous seems especially problematic. An example of a completely different interpretation of the same stratigraphic section was provided by Sageman et al. (2006) and Prokoph et al. (2001). They concluded that the dominant lithologic cycle in the Western Interior Pueblo section represents eccentricity and obliquity, respectively. Similarly, cyclostratigraphic estimates for the duration of OAE2 still vary by a factor of three. The time interval between the onset of the $\delta^{13}C$ excursion to the end of plateau is variously estimated as ~200 k.y. (Kuhnt et al., 1997, 2005), ~320 k.y. (Prokoph et al., 2001), ~400 k.y. (Caron et al., 1999), and ~600 k.y. (Sageman et al., 2006).

In the meantime, an accepted method to bypass inconclusive spectral results relies on visual interpretation of the cycle pattern. One of the inferred orbital cycles is projected onto a linear timescale; when done correctly, the resulting power spectra will yield other orbital cycles in the right configuration (Norris and Röhl, 1999; Shackleton et al., 1999; Wilson and Norris, 2001). However, an attempt to use this approach for the Leg 207 color data did not yield results that were easier to interpret than the power spectra against depth (Figs. **F3, F4, F5, F6,**

F7). Using inferred eccentricity minima as tie points for a linear timescale did remove the split peaks around the long cycle seen in most spectra (Figs. F3, F4, F5, F6, F7), which is no surprise, as those cycles were all forced onto the same wavelength. It did not enhance power in the precession range, nor did it shift spectral peaks closer to their expected position relative to the eccentricity cycle.

We therefore used the bandpass approach to try to determine which nonlinearities are present in the cycle pattern. If the eccentricity cycle is recognized correctly, the bandpass approach around the wavelength of the precession cycle should show the characteristic gradual increase–decrease in amplitude, with ~5 precession cycles bundled into each eccentricity cycle. Such waxing and waning in amplitude is indeed seen in Figures F3, F4, F5, F6, and F7. Comparison with long-term average sediment accumulation rates provides a further check on the consistency of the results, even though estimates for accumulation rates are very rough, because of the lack of precise age control. The Cenomanian, which lasted 6.1 m.y. (Gradstein et al., 2004), is ~60 m thick at Site 1260, indicating long-term average accumulation rates in the order of 1 cm/k.y. This translates to ~20 cm on average for precession cycles and 40 cm for obliquity if the sequence is complete without hiatuses. For the Turonian (4.2 m.y. duration) (Gradstein et al., 2004) at Site 1259 (~35 m thick) the long-term average accumulation rate is 0.8 cm/k.y., or 16 cm and 32 cm for precession cycle and obliquity cycles, respectively. Compared to long-term average accumulation rates, the thickness of the shortest cycle in the analyzed cores (Figs. F3, F4, F5, F6) is mostly somewhere in between values expected for precession and obliquity. The average thickness of the inferred precession cycles in the Turonian ranges from 15 cm in the upper half of Core 207-1260B-35R (Fig. F6), through 26 cm in Core 207-1259B-23R (Fig. F4), to 44 cm in Core 207-1259B-22R (Fig. F3). Cycle thicknesses in the Cenomanian are 33 cm in Core 207-1260B-37R (Fig. F4) and 25 cm within OAE2 in Core 207-1260B-35R (Fig. F6). To reconcile the cycle thickness distribution with the long-term average accumulation rates, it has to be assumed either that some of the cycle patterns represent obliquity rather than precession or that the Cenomanian and Turonian are incomplete. The former, that the cycle pattern is dominated by obliquity in some cores, is very unlikely, not only because of the five-to-one bundling of short and long cycles in all analyzed cores but also because it would imply that the long cycle represents some 200 k.y., which is not a value known from orbital fluctuations. The latter is more likely, that there are hiatuses, and that actual accumulation rates were higher than suggested by simple division of stratigraphic thickness by the duration of the entire Cenomanian or Turonian. A close comparison of trends in $\delta^{13}C$ values around OAE2 at Demerara Rise showed that there are indeed minor hiatuses (Erbacher et al., 2005), which we estimate to represent one or two precession cycles at most. More substantial hiatuses or condensed intervals could easily be present elsewhere within the mid-Cretaceous sequence, but they would be difficult to detect because of the lack of precise age control. For example, organic matter at Site 1260 is more degraded in the lowest part of the Cenomanian sequence below ~445 meters composite depth (mcd) (Erbacher, Mosher, Malone, et al., 2004), an interval where foraminiferal packstones are the dominant lithology. The combination points to extensive winnowing and long exposure times at the seafloor, suggesting that accumulation of sediment was slow or intermittent. Similarly, the glauconitic/phosphatic packstones,

which occur in the Turonian at all three shallow-water sites, could be associated with a condensed sequence.

As far as interpretation of the link between climate and sediment supply is concerned, the main implication of our interpretation of cycle patterns is that sedimentation rates vary by a factor of two or more within a single core but that it depends on the type of sediment how the variation relates to orbital cycles. Although our data set is not large enough to be entirely conclusive, it appears that the variation is predictable in most pelagic sediments but not so in intervals with planktonic foraminiferal packstones. Within pelagic intervals, the correlation between bed thickness and b* (carbonate content) can be positive (Fig. F3) as well as negative (Fig. F6). We relate the different correlation patterns to variable response of carbonate and lithogenic sedimentation rates to climate cycles that is dependent on the actual depositional environment.

Core 207-1259B-22R, with pelagic carbonate-rich layers, shows a strong positive correlation between cycle length and b* (Fig. F3). The correlation can be explained by a combination of increased carbonate accumulation and reduced compaction during high-amplitude precession cycles. Comparison of thin sections from organic-rich and pelagic carbonate-rich sediments shows that fecal pellets are thicker (i.e., less compacted) in carbonate-rich levels. The examples in Plate P3, figures 2 and 7, from the Tarfaya Basin illustrate this for the same type of fecal pellet, which suggests that in this case the difference is because of early diagenetic carbonate precipitation. On the other hand, the compositional difference in fecal pellets from carbonate-poor and carbonate-rich environments will be reflected in degree of compaction, in the sense that a fecal pellet full of coccoliths cannot be compressed as much as one that consists of organic matter and clay only. Systematic measurements of fecal pellet size may reveal how strong compaction and diagenetic lithification effects are; our qualitative assessment at this stage is that they cannot account for the entire variation in bed thickness. We therefore suggest that there is substantial variation in carbonate accumulation rates in response to precession cycles, with maximum carbonate accumulation during strong precession maxima or minina.

Core 207-1260B-35R shows a negative correlation between b* and the thickness of precession cycles if two carbonate concretions and one exceptionally thin cycle are excluded (Fig. F6). The difference with Core 207-1259B-22R is that sedimentation rates are much lower in Core 207-1260B-35R (1.3 and 0.7 cm/k.y., Fig. F6, vs. 2.5 cm/k.y. in Core 207-1259B-22R, Fig. F3). In addition, low b* values point to low carbonate content. A limited number of shipboard analyses are available, which give carbonate content values of generally <30 wt% for Cores 207-1260B-35R and 34R and the corresponding interval in Hole 1260A. Samples from the same interval show that planktonic foraminifers are rare but that they are well preserved where present. This suggests that low carbonate content is largely due to low carbonate productivity and not to dissolution. TOC content is too low (~7 wt% on average) (Erbacher, Mosher, Malone, et al., 2004) to account for much variation in accumulation rates. Variation in the siliciclastic contribution is therefore the most probable candidate. This suggests that thick precession cycles, which have low carbonate content, are formed as the result of increased dilution by terrigenous fluxes.

The lack of a consistent correlation between bed thickness and carbonate content in intervals with planktonic foraminiferal packstones (Figs. F4, F5) is most likely related to selective removal of material due

to winnowing in carbonate-rich levels. Planktonic foraminiferal packstones cannot be formed by normal pelagic sedimentation. Planktonic foraminifers are secondary producers, and the total biomass higher in the food chain is usually much lower than that of primary producers. Coccoliths, the remains of primary producers, are much more abundant in pelagic Cretaceous sediments than are planktonic foraminifers. Furthermore, the packstones contain few of the small specimens that are abundant in the pelagic carbonate-rich levels. A living population of planktonic foraminifers in the surface water is characterized by an exponential decrease in numbers of specimens during growth due to mortality, with the result that a seafloor population is dominated by preadult specimens (Peeters et al., 1999). Such small specimens can be removed through dissolution, but this results in very low numbers of specimens within the sediment, as insoluble components are selectively enriched. The high concentrations of foraminifers in the packstones as well as the near-absence of a fine-grained matrix in many samples (e.g., Pl. **P2,** fig. 2) therefore point to size-sorting by physical processes. Such size-sorting can be produced by turbidity currents. However, the packstone laminae lack the sharp base and fining-upward sequence that would be expected in turbidites. The semiregular alternation between pelagic and packstone laminae (Pl. **P1,** figs. 5, 6) and the occasional presence of low-angle cross-stratification are best explained by in situ winnowing. Whether this is because of current action or to wave action above storm wave base is difficult to distinguish. Either way, the cyclic distribution pattern of the packstones indicates that energy levels at the seafloor fluctuated in response to orbital cycles. The implication for the bed thickness pattern is that sedimentation rates are determined by two opposing processes: carbonate production and sediment removal. The variable correlation between cycle thickness and carbonate content from weakly positive to strongly negative (Figs. **F4, F5**) could well reflect variable degrees of winnowing.

Overall, the strong and often systematic variability in precession cycle thickness can explain the weak power in the precession frequency range in power spectra against depth. How the possible obliquity cycle fits into the pattern is not entirely clear from the spectral results only. Most power spectra (Figs. **F3, F5, F6, F7**) show some sign of (slightly) enhanced power in the expected obliquity range. However, the expected pattern for an obliquity cycle is that it has virtually constant amplitude over time. In contrast, the bandpass filter around this frequency usually shows high amplitude only for the occasional very thick carbonate-rich interval but is low amplitude elsewhere. In some cases, this thick carbonate interval shows signs of a double peak (e.g., the one at 437.8 mbsf in Fig. **F5**), but mostly the "obliquity bandpass filter" picks out individual cycles that fit well with the precession pattern. The correlation with the Tarfaya Basin suggests a possible explanation for the role of the obliquity cycle.

The cycle pattern in the Tarfaya Basin differs from Demerara Rise in having a strong obliquity cycle and weak precession–eccentricity components (Kuhnt et al., 1997), even though individual beds in and around OAE2 can be correlated between the two areas. The obliquity cycle in the Tarfaya Basin was related to trade wind–induced upwelling (Kuhnt et al., 1997, 2005), but this explanation becomes less likely in the light of the weak obliquity cycle at Demerara Rise. Synchronous carbonate cycles during OAE2 suggest that both regions are part of the same climate system. To explain the difference in the cycle patterns, two different processes are required that acted on both areas simulta-

neously but with different impact on sediment accumulation. The main lithologic difference between the two regions is the presence of terrigenous material at Demerara Rise (Erbacher, Mosher, Malone, et al., 2004) and its near-absence in the Tarfaya Basin (Kuhnt et al., 1997). Another difference is that the entire mid-Cretaceous record at Demerara Rise is laminated, pointing to the continuous presence of fully anoxic conditions, whereas the Tarfaya record contains bioturbated carbonate-rich beds especially before and after OAE2. The simplest explanation for the distinct cycle patterns in the Tarfaya Basin and at Demerara Rise is therefore that the obliquity cycle represents ventilation of the oxygen minimum zone (OMZ), whereas the eccentricity–precession couple represents regional atmospheric circulation. A ventilation signal may have been generated elsewhere in the North Atlantic (e.g., through intermediate water formation in the high latitudes) and transported to the equator. Any fluctuations in preformed oxygen content in the subsurface would have had little impact on Demerara Rise. Apparently, any oxygen in the subsurface was consumed long before it reached the area. The presence of bioturbation in the Tarfaya Basin, which is closer to the more continuously oxic central North Atlantic to the north, indicates that this area was more sensitive to changes in subsurface oxygen content. Atmospheric circulation would have impact on upwelling intensity as well as average annual rainfall. A precession cycle in rainfall and runoff would have had no impact at all in the Tarfaya Basin, as there is no terrigenous material to register the signal. Precession cycle–induced fluctuations in upwelling intensity could have been of minor importance in the Tarfaya Basin, if composition of the upwelling water (ventilation) is more important than upwelling intensity.

High accumulation rates of organic matter in the wider region are generally attributed to upwelling (e.g., Erbacher, Mosher, Malone, et al., 2004; Kuhnt et al., 1997, 2005). By inference, the carbonate-rich–organic-rich sediment cycles result from orbital-scale changes in wind strength and/or location of the trade wind zone, similar to glacial–interglacial fluctuations during the Quaternary in the same region (e.g., Peterson et al., 2000). Wind-driven upwelling was undoubtedly of importance along the equatorial North Atlantic margin, given the geometry of the coast line and its paleolatitude within the influence of the trade wind system (Kruijs and Barron, 1990). Features in the texture of the sediment suggest that productivity was strongly seasonal, which in low latitudes is usually related to seasonal upwelling. The abundance of fecal pellets with monospecific coccolith floras in the Tarfaya Basin (Pl. **P3,** figs. 2–4) point to the occurrence of sudden blooms in the surface water. The presence of lamina couplets in Core 207-1259B-23R is suggestive of alternation between wet and upwelling seasons (Pl. **P1,** fig. 8). Average sedimentation rates in this core of 1.4 cm/k.y. (Fig. **F4**) or 14 µm/yr are too low to expect persistent preservation of varves, but the lamina couplets, which are ~100 µm thick, could represent an annual sequence during years with higher than average sedimentation rates and/or exceptional preservation.

Even though it is likely that both Demerara Rise and the Tarfaya Basin represent high-productivity upwelling settings in general, there is little or no direct evidence to indicate which part of the carbonate-rich–organic-rich cycles represents the highest surface water productivity. The carbonate part of the cycles certainly represents the highest carbonate productivity, but whether this corresponds to high total productivity in the surface water is not clear. In the modern ocean, pelagic carbonate production is generally highest under mesotrophic condi-

tions (Brummer and van Eijden, 1992); diatoms become more abundant under high-productivity conditions. The analog suggests that carbonate-rich beds in the mid-Cretaceous represent intermediate surface water productivity. On the other hand, diatoms did exist during the Cretaceous, but there is no evidence that they were numerically important. Lack of competition by biosiliceous primary producers may have meant that carbonate producers could dominate under high-productivity conditions as well as under mesotrophic conditions. Independent measures of how productivity varied within a precession cycle may be difficult to find. Sedimentation rates can be estimated for one entire precession cycle at best; therefore, any productivity indicator based on sedimentation rates can only give an average for one entire cycle but cannot account for variation within that cycle. The planktonic foraminiferal assemblages in the mid-Cretaceous at Demerara Rise consist virtually entirely of globular forms, which is indicative of some form of exceptional nonopen oceanic surface water conditions, but there is no direct evidence whether this is related to high surface water productivity or to a very shallow OMZ impinging on the habitat of deep-dwelling species. The distribution of radiolarians relative to planktonic foraminifers may have provided some information about productivity conditions, but the primary distribution of radiolarians is overprinted too strongly by diagenetic dissolution and/or migration of the silica.

The most significant feature at Demerara Rise that might help to understand the cyclic pattern could well turn out to be the distribution of the planktonic foraminiferal packstones. Their distribution is at least partly regular relative to orbital climate cycles. The inferred amalgamation of three packstone cycles in the lower part of Core 207-1260B-37R (Fig. **F5**) implies that energy levels near the seafloor remained high enough to cause winnowing for a period of ~60 k.y. alternating with ~40-k.y.-long deposition of fine-grained material, a pattern that is difficult to explain as related to orbital cycles. On the other hand, packstone layers in the upper part of the same core (Fig. **F5**) as well as in Core 207-1259B-23R (Fig. **F4**) exhibit a strong precession signature, showing that winnowing was controlled by climate cycles under the right conditions. The stratigraphic distribution of the packstone layers indicates that they represent a (relatively) shallow water depth (Fig. **F2**). They are most abundant in the lower part of the mid-Cretaceous sequence at Sites 1259–1261 after subsidence started, and they persist longer in the shallowest sites (1259 and 1261) where pelagic sedimentation started later. From the size distribution of the planktonic foraminifers, it can be inferred that packstone layers correspond to pelagic carbonate layers in the deepwater sites. Winnowing can concentrate large foraminiferal specimens only if they are present in the first place. Organic-rich layers at all sites are dominated by small specimens, whatever the paleowater depth. Large planktonic foraminiferal specimens are abundant only in the planktonic foraminiferal packstones and in pelagic carbonate-rich levels.

The presence of the foraminiferal packstones, because they represent increased energy levels at the seafloor at shallow depths, implies that any upwelling was most intense during periods of high carbonate sedimentation rates. The winnowing may have been wave induced or current induced; a decisive distinction between the two is difficult. If wave induced, they should represent deepening of storm wave base, as Demerara Rise must have been below regular wave base to be able to maintain anoxic conditions over long periods of time. If current induced,

they almost certainly represent strengthening of currents in the surface to shallow subsurface ocean. The stratigraphic distribution of packstones right from the base of the organic-rich unit makes it unlikely that deep currents were involved. Because of the close correlation between surface water circulation and wind stress (Munk, 1950), both explanations for the winnowing imply that atmospheric and oceanic circulation, and therefore upwelling intensity, were more vigorous during deposition of carbonate-rich layers. This in turn implies that the high organic carbon content of organic-rich layers is induced primarily by the presence of enhanced anoxia, whatever the ultimate effect on oceanic productivity.

ACKNOWLEDGMENTS

This research used samples and data provided by the Ocean Drilling Program (ODP). ODP is sponsored by the U.S. National Science Foundation (NSF) and participating countries under management of Joint Oceanographic Institutions (JOI), Inc. The help of W. Hale and A. Wuelbers with sample collection in the Bremen ODP repository is much appreciated.

REFERENCES

Arthur, M.A., Schlanger, S.O., and Jenkyns, H.C., 1987. The Cenomanian–Turonian oceanic anoxic event, II. Palaeoceanographic controls on organic-matter production and preservation. *In* Brooks, J., and Fleet, A.J. (Eds.), *Marine Petroleum Source Rocks*. Geol. Soc. Spec. Publ., 26:401–420.

Berger, A.L., 1978. Long-term variations of daily insolation and Quaternary climatic changes. *J. Atmos. Sci.,* 35(12):2362–2367. **doi:10.1175/1520-0469(1978)035<2362:LTVODI>2.0.CO;2**

Berger, A.L., Loutre, M.F., and Dehant, V., 1989. Influence of the changing lunar orbit on the astronomical frequencies of pre-Quaternary insolation patterns. *Paleoceanography,* 4:555–564.

Brummer, G.J.A., and van Eijden, A.J.M., 1992. "Blue-ocean" paleoproductivity estimates from pelagic carbonate mass accumulation rates. *Mar. Micropaleontol.,* 19(1–2):99–117. **doi:10.1016/0377-8398(92)90023-D**

Calvert, S.E., 1987. Oceanographic controls on the accumulation of organic matter in marine sediments. *In* Brooks, J., and Fleet, A.J. (Eds.), *Marine Petroleum Source Rocks*. Geol. Soc. Spec. Publ., 26:137–151.

Caron, M., Robaszynski, F., Amedro, F., Baudin, F., Deconinck, J.F., Hochuli, P.A., von Salis-Perch Nielsen, K., and Tribovillard, N., 1999. Estimation de la duree de l'evenement anoxique global au passage Cenomanien/Turonien; approche cyclostratigraphique dans la formation Bahloul en Tunisie centrale. *Bull. Soc. Geol. Fr.,* 170:145–160.

Erbacher, J., Friedrich, O., Wilson, P.A., Birch, H., and Mutterlose, J., 2005. Stable organic carbon isotope stratigraphy across Oceanic Anoxic Event 2 of Demerara Rise, western tropical Atlantic. *Geochem., Geophys., Geosyst.,* 6(6):Q06010. **doi:10.1029/2004GC000850**

Erbacher, J., Huber, B.T., Norris, R.D., and Markey, M., 2001. Increased thermohaline stratification as a possible cause for an ocean anoxic event in the Cretaceous period. *Nature (London, U. K.),* 409(6818):325–327. **doi:10.1038/35053041**

Erbacher, J., Mosher, D.C., Malone, M.J., et al., 2004. *Proc. ODP, Init. Repts.,* 207: College Station, TX (Ocean Drilling Program). **doi:10.2973/odp.proc.ir.207.2004**

Erlich, R.N., Macsotay, I.O., Nederbragt, A.J., and Lorente, M.A., 1999. Palaeoecology, palaeogeography and depositional environments of Upper Cretaceous rocks of western Venezuela. *Palaeogeogr., Palaeoclimatol., Palaeoecol.,* 153(1–4):203–238. **doi:10.1016/S0031-0182(99)00072-3**

Gradstein, F.M., Ogg, J.G., and Smith, A. (Eds.), 2004. *A Geologic Time Scale 2004:* Cambridge (Cambridge Univ. Press).

Imbrie, J., 1985. A theoretical framework for the Pleistocene ice ages. *J. Geol. Soc. (London, U. K.),* 142:417–432.

Kruijs, E., and Barron, E., 1990. Climate model prediction of paleoproductivity and potential source rock distribution. *In* Huc, A.Y. (Ed.), *Deposition of Organic Facies*. AAPG Stud. Geol., 30:195–216.

Kuhnt, W., Herbin, J.P., Thurow, J., and Wiedmann, J., 1990. Distribution of Cenomanian–Turonian organic facies in the western Mediterranean and along the adjacent Atlantic margin. *In* Huc, A.Y. (Ed.), *Deposition of Organic Facies*. AAPG Stud. Geol., 30:133–160.

Kuhnt, W., Luderer, F., Nederbragt, S., Thurow, J., and Wagner, T., 2005. Orbital-scale record of the late Cenomanian–Turonian oceanic anoxic event (OAE-2) in the Tarfaya Basin (Morocco). *Int. J. Earth Sci.,* 94(1):147–159. **doi:10.1007/s00531-004-0440-5**

Kuhnt, W., Nederbragt, A., and Leine, L., 1997. Cyclicity of Cenomanian–Turonian organic-carbon-rich sediments in the Tarfaya Atlantic coastal basin (Morocco). *Cretaceous Res.,* 18(4):587–601. **doi:10.1006/cres.1997.0076**

Kuypers, M.M.M., Pancost, R.D., Nijenhuis, I.A., and Sinninghe Damsté, J.S., 2002. Enhanced productivity led to increased organic carbon burial in the euxinic North Atlantic basin during the late Cenomanian oceanic anoxic event. *Paleoceanography,* 17(4):1051. **doi:10.1029/2000PA000569**

Munk, W.H., 1950. On the wind-driven ocean circulation. *J. Meteorol.,* 7:79–93.

Nederbragt, A.J., 1999. Quantitative biogeography of Cretaceous planktonic foraminifera from the North Atlantic and circum-Mediterranean. *Neues Jahrb. Geol. Palaeontol., Abh.,* 212:263–288.

Nederbragt, A.J., Fiorentino, A., and Klosowska, B., 2001. Quantitative analysis of calcareous microfossils across the Albian–Cenomanian boundary oceanic anoxic event at DSDP Site 547 (North Atlantic). *Palaeogeogr., Palaeoclimatol., Palaeoecol.,* 166(3–4):401–421. **doi:10.1016/S0031-0182(00)00227-3**

Nederbragt, A.J., and Thurow, J.W., 2004. Digital sediment colour analysis as a method to obtain high resolution climate proxy records. *In* Francus, P. (Ed.), *Image Analysis, Sediments, and Paleoenviroments*. Dev. Paleoenviron. Res., 7:105–124.

Norris, R.D., and Röhl, U., 1999. Carbon cycling and chronology of climate warming during the Palaeocene/Eocene transition. *Nature (London, U. K.),* 401(6755):775–778. **doi:10.1038/44545**

Peeters, F., Ivanova, E., Conan, S., Brummer, G.-J., Ganssen, G., Troelstra, S., and van Hinte, J., 1999. A size analysis of planktic foraminifera from the Arabian Sea. *Mar. Micropaleontol.,* 36(1):31–63. **doi:10.1016/S0377-8398(98)00026-7**

Peterson, L.C., Haug, G.H., Hughen, K.A., and Röhl, U., 2000. Rapid changes in the hydrologic cycle of the tropical Atlantic during the last glacial. *Science,* 290(5498):1947–1951. **doi:10.1126/science.290.5498.1947**

Paillard, D., Labeyrie, L., and Yiou, P., 1996. Macintosh program performs time-series analysis. *Eos, Trans. Am. Geophys. Union,* 77(39):379. **doi:10.1029/96EO00259**

Pike, J., and Kemp, A.E.S., 1996. Records of seasonal flux in Holocene laminated sediments from the Gulf of California. *In* Kemp, A.E.S. (Ed.), *Palaeoecology and Palaeoceanography from Laminated Sediments*. Geol. Soc. Spec. Publ., 116:157–169.

Press, W.H., Teukolsky, S.A., Vetterling, W.T., and Flannery, B.P., 1992. *Numerical Recipes in C:* Cambridge (Cambridge Univ. Press).

Prokoph, A., Villeneuve, M., Agterberg, F.P., and Rachold, V., 2001. Geochronology and calibration of global Milankovitch cyclicity at the Cenomanian–Turonian boundary. *Geology,* 29(6):523–526. **doi:10.1130/0091-7613(2001)029<0523:GACOGM>2.0.CO;2**

Ravilious, K., 2002. Controls on mid-Cretaceous marine sedimentation in the Tarfaya Basin, southern Morocco [Ph.D. thesis]. Univ. London.

Roth, P.H., and Krumbach, K.R., 1986. Middle Cretaceous calcareous nannofossil biogeography and preservation in the Atlantic and Indian Oceans: implications for paleoceanography. *Mar. Micropaleontol.,* 10(1–3):235–266. **doi:10.1016/0377-8398(86)90031-9**

Sageman, B.B., Meyers, S.R., and Arthur, M.A., 2006. Orbital time scale and new C-isotope record for Cenomanian–Turonian boundary stratotype. *Geology,* 34(2):125–128. **doi:10.1130/G22074.1**

Schaaf, M., and Thurow, J., 1994. A fast and easy method to derive highest-resolution time-series datasets from drillcores and rock samples. *Sediment. Geol.,* 94(1–2):1–10. **doi:10.1016/0037-0738(94)90143-0**

Schlanger, S.O., and Jenkyns, H.C., 1976. Cretaceous oceanic anoxic events: causes and consequences. *Geol. Mijnbouw,* 55:179–184.

Shackleton, N.J., Crowhurst, S.J., Weedon, G.P., and Laskar, J., 1999. Astronomical calibration of Oligocene–Miocene time. *In* Shackleton N.J., McCave, I.N., and Graham, P.W. (Eds.), *Astronomical (Milankovitch) Calibration of the Geological Time-Scale.* Philos. Trans. R. Soc., Ser. A., 357(1757):1907–1929. **doi:10.1098/rsta.1999.0407**

Shackleton, N.J., and Opdyke, N.D., 1973. Oxygen isotope and paleomagnetic stratigraphy of equatorial Pacific core V28-238: oxygen isotope temperatures and ice volumes on a 10^5 year and 10^6 year scale. *Quat. Res.,* 3(1):39–55. **doi:10.1016/0033-5894(73)90052-5**

Stein, R., 1986. Organic carbon and sedimentation rate—further evidence for anoxic deep-water conditions in the Cenomanian/Turonian Atlantic Ocean. *Mar. Geol.,* 72(3–4):199–209. **doi:10.1016/0025-3227(86)90119-2**

Thurow, J., 1988. Diagenetic history of Cretaceous radiolarians, North Atlantic Ocean (ODP Leg 103 and DSDP Holes 398D and 603B). *In* Boillot, G., Winterer, E.L., et al., *Proc. ODP, Sci. Results,* 103: College Station, TX (Ocean Drilling Program), 531–555. **doi:10.2973/odp.proc.sr.103.182.1988**

Thurow, J., Moullade, M., Brumsack, H.-J., Masure, E., Taugourdeau-Lantz, J., and Dunham, K., 1988. The Cenomanian/Turonian boundary event (CTBE) at Hole 641A, ODP Leg 103 (compared with the CTBE interval at Site 398). *In* Boillot, G., Winterer, E.L., et al., *Proc. ODP, Sci. Results,* 103: College Station, TX (Ocean Drilling Program), 587–634. **doi:10.2973/odp.proc.sr.103.172.1988**

Wilson, P.A., and Norris, R.D., 2001. Warm tropical ocean surface and global anoxia during the mid-Cretaceous period. *Nature (London, U. K.),* 412(6845):425–429. **doi:10.1038/35086553**

Figure F1. Paleogeographic reconstruction at 100 Ma (latest Albian) showing localities discussed in the text, with enlargement of modern location of Leg 207 sites on Demerara Rise and of selected drill cores (triangles) and a quarry (square) in the Tarfaya Basin (after Kuhnt et al., 1997).

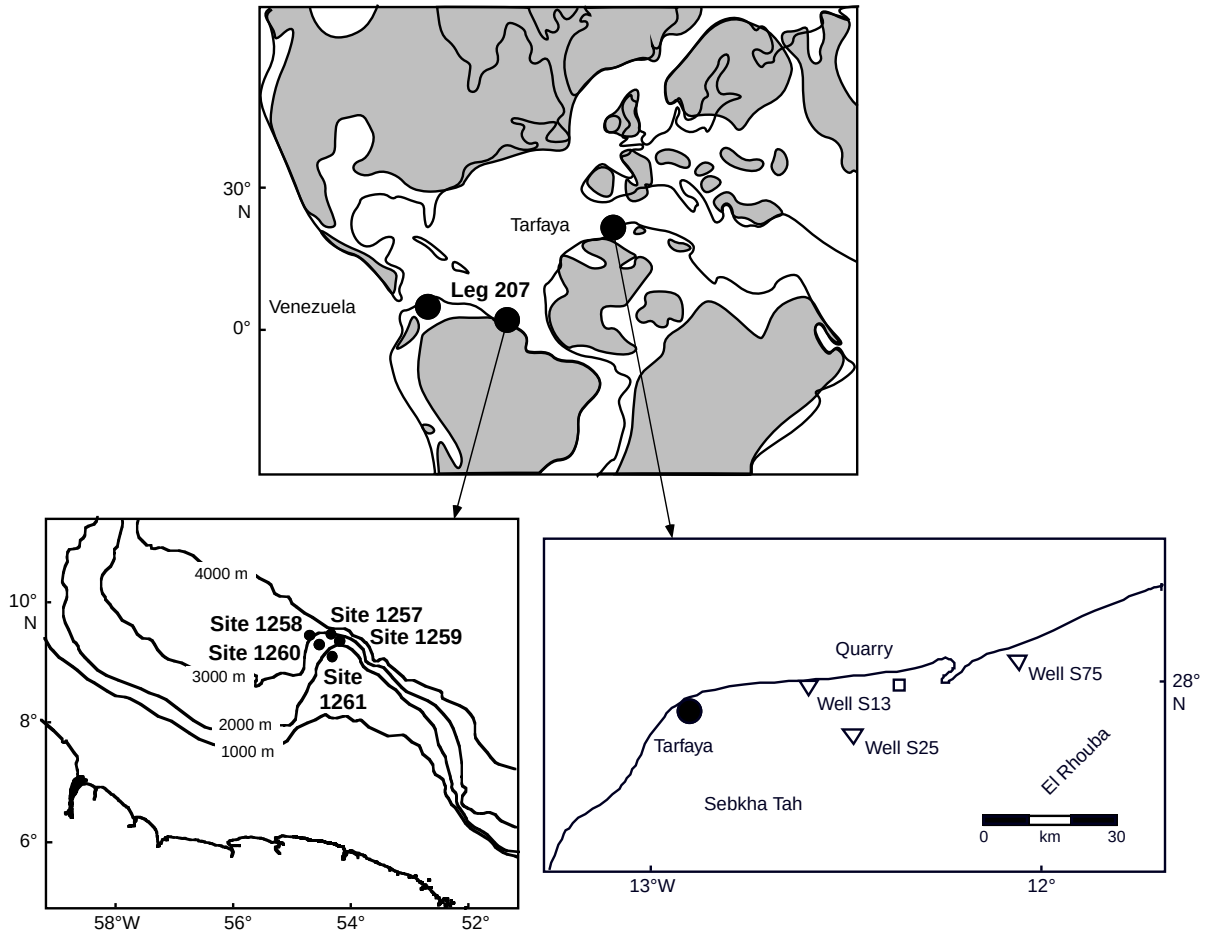

Figure F2. Schematic distribution of major lithologies in the mid-Cretaceous unit at Sites 1258–1261 on Demerara Rise and in Well S13 in the Tarfaya Basin. The stratigraphic range of Ocean Anoxic Event 2 (OAE2) is from Erbacher et al. (2005) and Kuhnt et al. (2005). The lithology at Site 1257 is similar to that at Site 1258. Note that the distribution of diagenetic carbonates is not indicated; they are present at all sites but their stratigraphic distribution appears irregular.

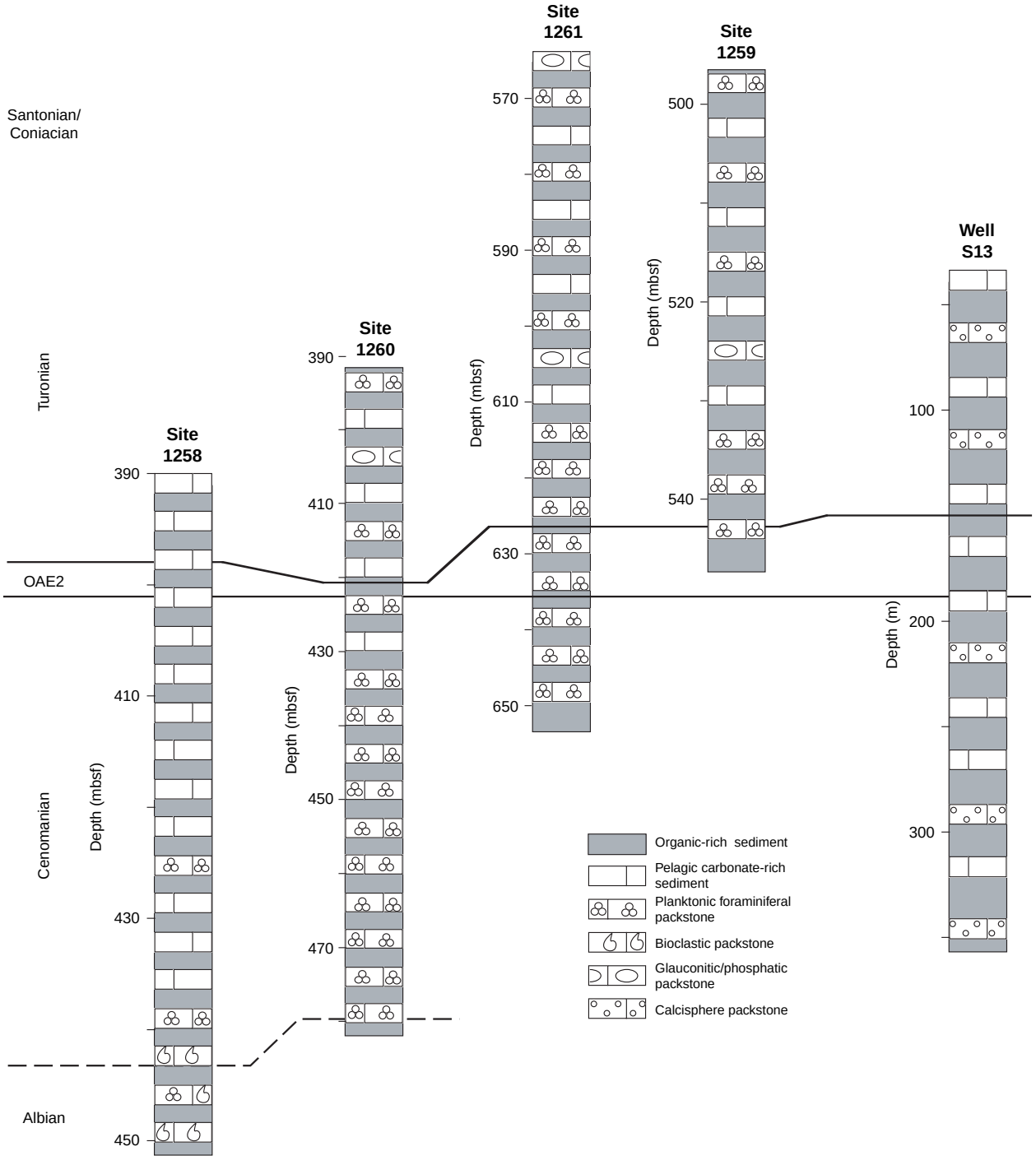

Figure F3. Cycle pattern in Core 207-1259B-22R (Turonian). **A.** b* time series with low-pass and bandpass filters around the expected wavelengths of the eccentricity, precession, and obliquity cycles. Numbers along filtered series indicate the band of the filter in meters. High b* values represent pelagic limestones, unless marked otherwise. PF = planktonic foraminiferal packstone, C = level with carbonate concretions. **B.** Blackman-Tukey power spectrum of b* time series. Numbers refer to the wavelength in meters of the main spectral peaks. Connected vertical lines indicate expected position of precession peaks assuming the highest peak represents eccentricity. b.w. = bandwidth. **C.** Crossplot of cycle thickness derived from the precession bandpass filter against the average b* value for the corresponding interval, with linear correlation coefficient (*r*) shown in plot; the average thickness of the inferred precession cycles is 44 cm.

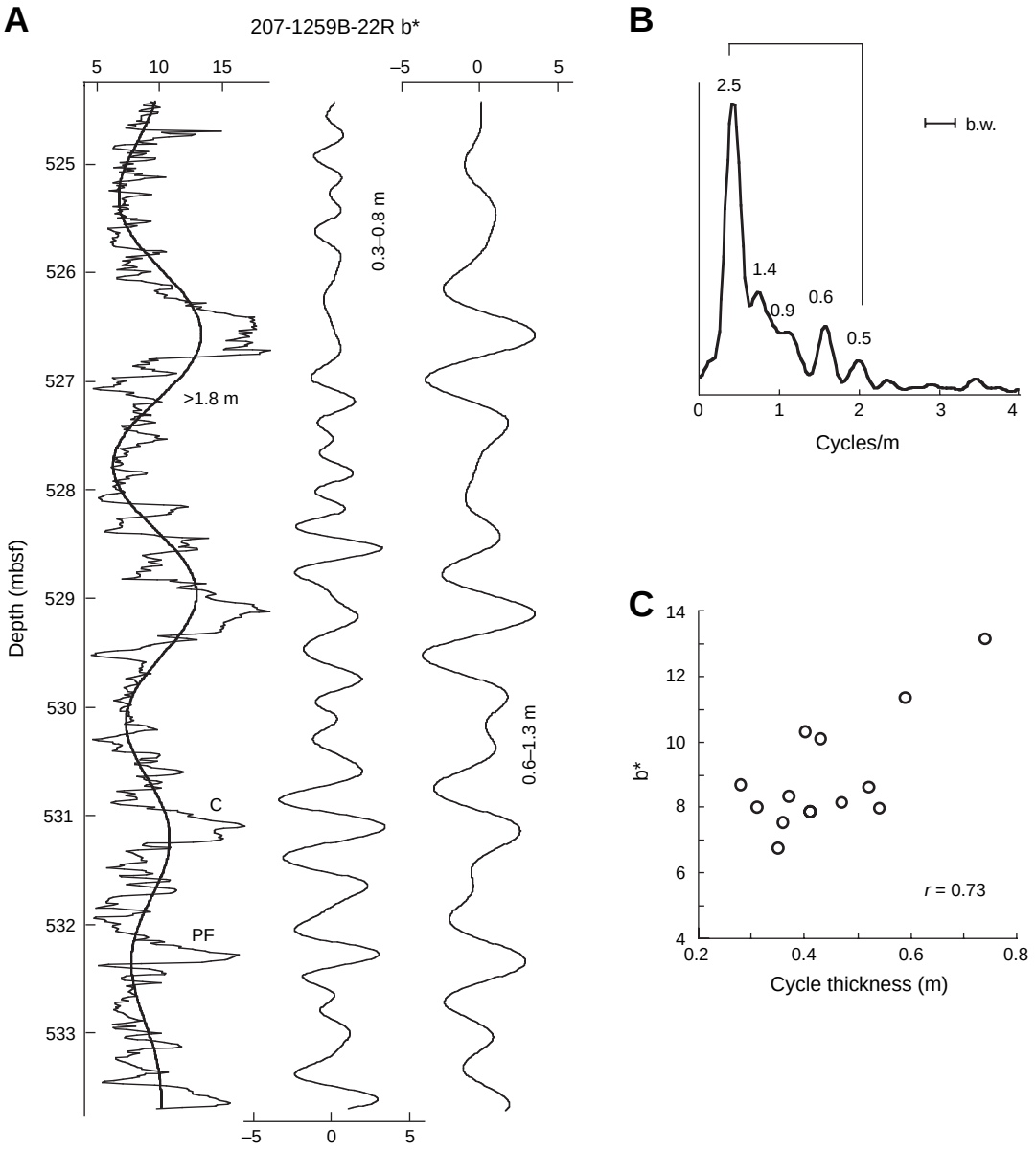

Figure F4. Cycle pattern in Core 207-1259B-23R (Turonian). **A.** b* time series with low-pass and bandpass filters around the expected wavelengths of the eccentricity, precession, and obliquity cycles. PF = planktonic foraminiferal packstone, C = level with carbonate concretions. **B.** Blackman-Tukey power spectrum of b* time series. b.w. = bandwidth. **C.** Crossplot of cycle thickness derived from the precession bandpass filter against the average b* value for the corresponding interval. The average precession-cycle thickness is 26 cm. For further explanation see Figure F3, p. 23.

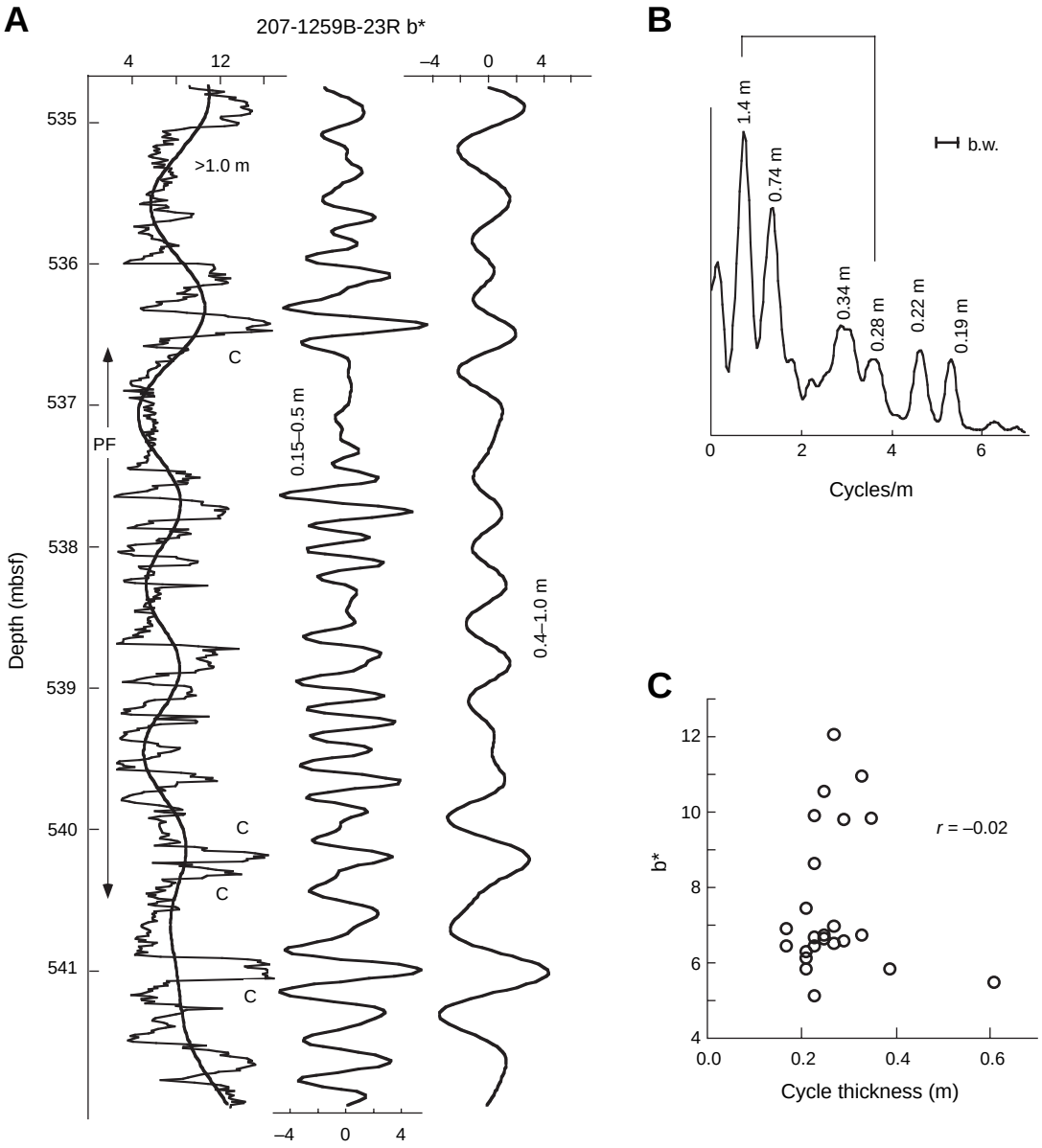

Figure F5. Cycle pattern in Core 207-1260B-37R (Cenomanian). **A.** b* time series with low-pass and bandpass filters around the expected wavelengths of the eccentricity, precession, and obliquity cycles. Note that all carbonate-rich levels in this core are planktonic foraminiferal packstones. **B.** Blackman-Tukey power spectrum of b* time series. The two connected vertical lines indicate expected position of precession peaks assuming both high peaks represent eccentricity cycles with different sedimentation rates. b.w. = bandwidth. **C.** Crossplot of cycle thickness derived from the precession bandpass filter against the average b* value for the corresponding interval. The average thickness of the inferred precession cycles is 33 cm. For further explanation see Figure F3, p. 23.

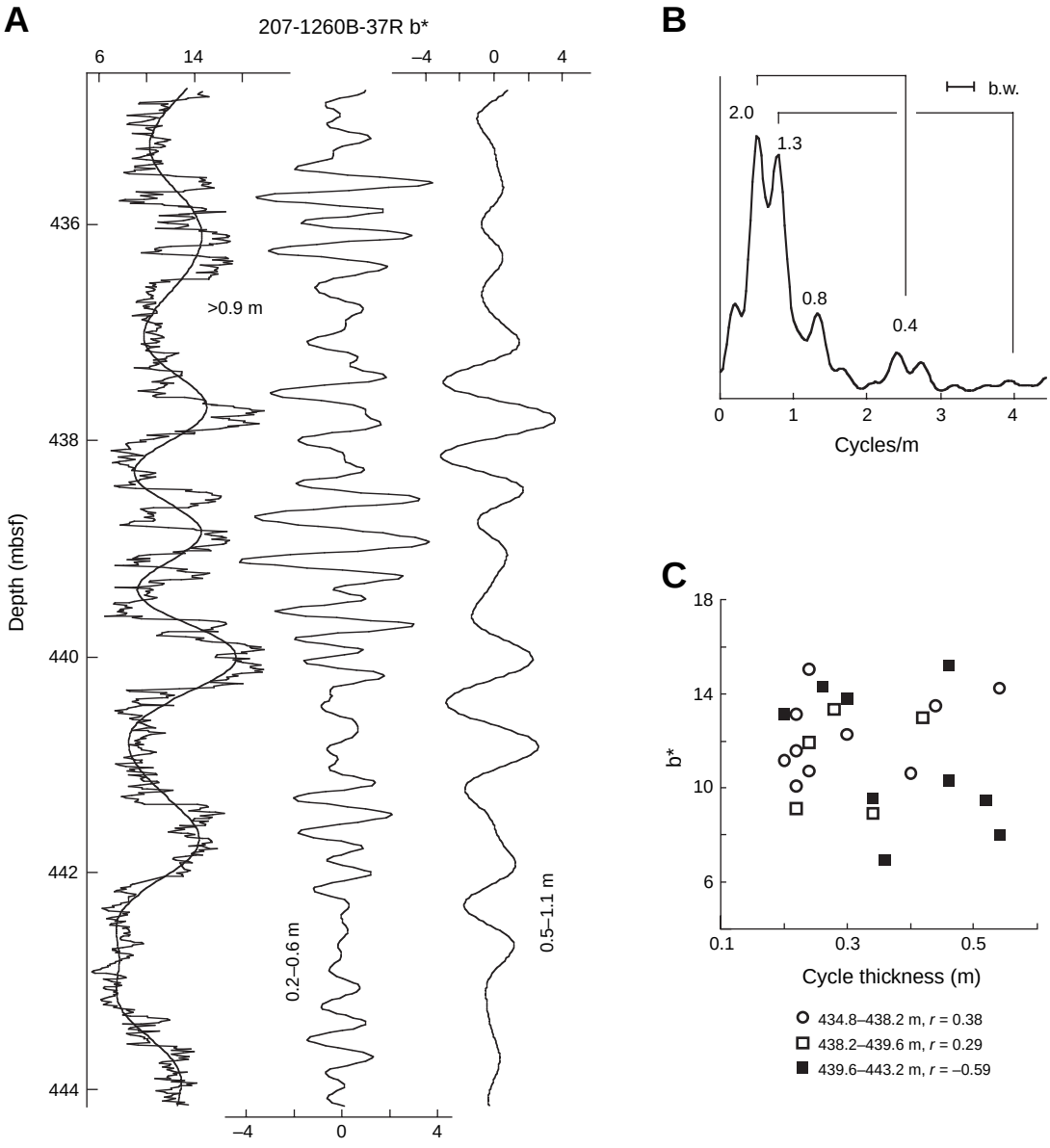

Figure F6. Cycle pattern in Core 207-1260B-35R (OAE2 and lower Turonian). **A.** b* time series with low-pass and bandpass filters around the expected wavelengths of the eccentricity, precession, and obliquity cycles. Horizontal lines mark (i) onset of $\delta^{13}C$ excursion, (ii) end of plateau, and (iii) short-lasting regional excursion after OAE2 (Erbacher et al., 2005). Note change in cycle thickness at 422 mcd. **B.** Blackman-Tukey power spectrum of b* time series. b.w. = bandwidth. **C.** Crossplot of cycle thickness derived from the precession bandpass filter against the average b* value for the corresponding interval. Symbols marked with an asterisk (*) were excluded from correlation coefficient. The average thickness of precession cycles below and above 422 mcd is 25 cm and 15 cm, respectively. For further explanation see Figure F3, p. 23.

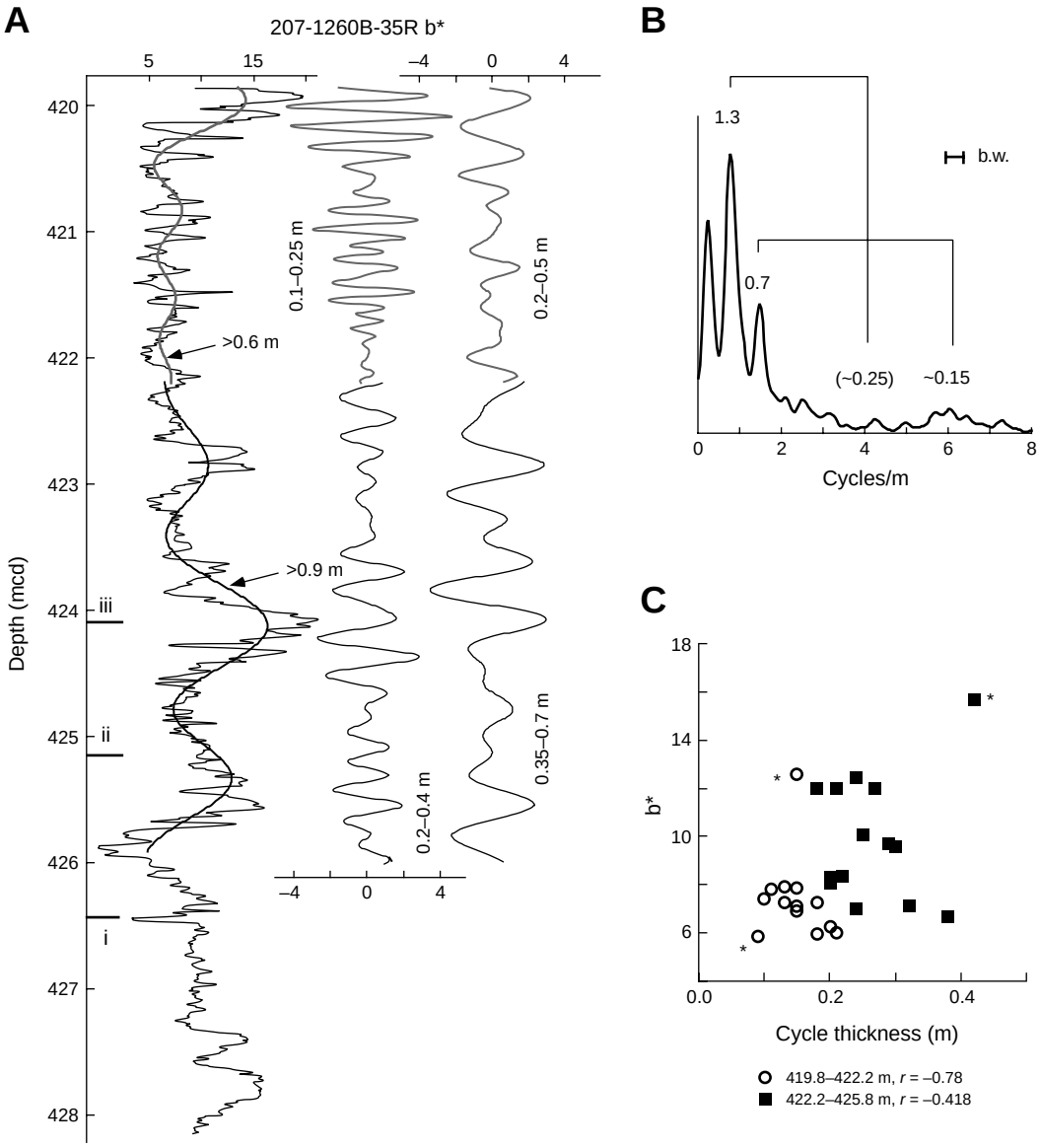

Figure F7. Cycle pattern in Core 207-1258A-42R (OAE2 and Lower Turonian). **A.** Core 207-1260B-35R as in Figure F6, p. 26, to illustrate close similarity of color records. Black horizontal lines mark correlation based on published $\delta^{13}C$ stratigraphy (Erbacher et al., 2005) indicating (i) onset of excursion, (ii) end of plateau, and (iii) short-lasting regional excursion after OAE2. Further dashed lines indicate visual correlation of color pattern. **B.** b* time series for Core 207-1258A-42R with low-pass and bandpass filters around the expected wavelengths of the eccentricity, precession, and obliquity cycles. Core 207-1257C-17R is shown to illustrate continuation of cycle pattern lower in the section. Note that our interpretation of the end of the excursion plateau (see Fig. F8, p. 28) differs from that presented in Erbacher et al. (2005), based on the comparison with Core 207-1260B-35R. **C.** Blackman-Tukey power spectrum of b* time series in Core 207-1258A-42R. b.w. = bandwidth. For further explanation see Figure F3, p. 23.

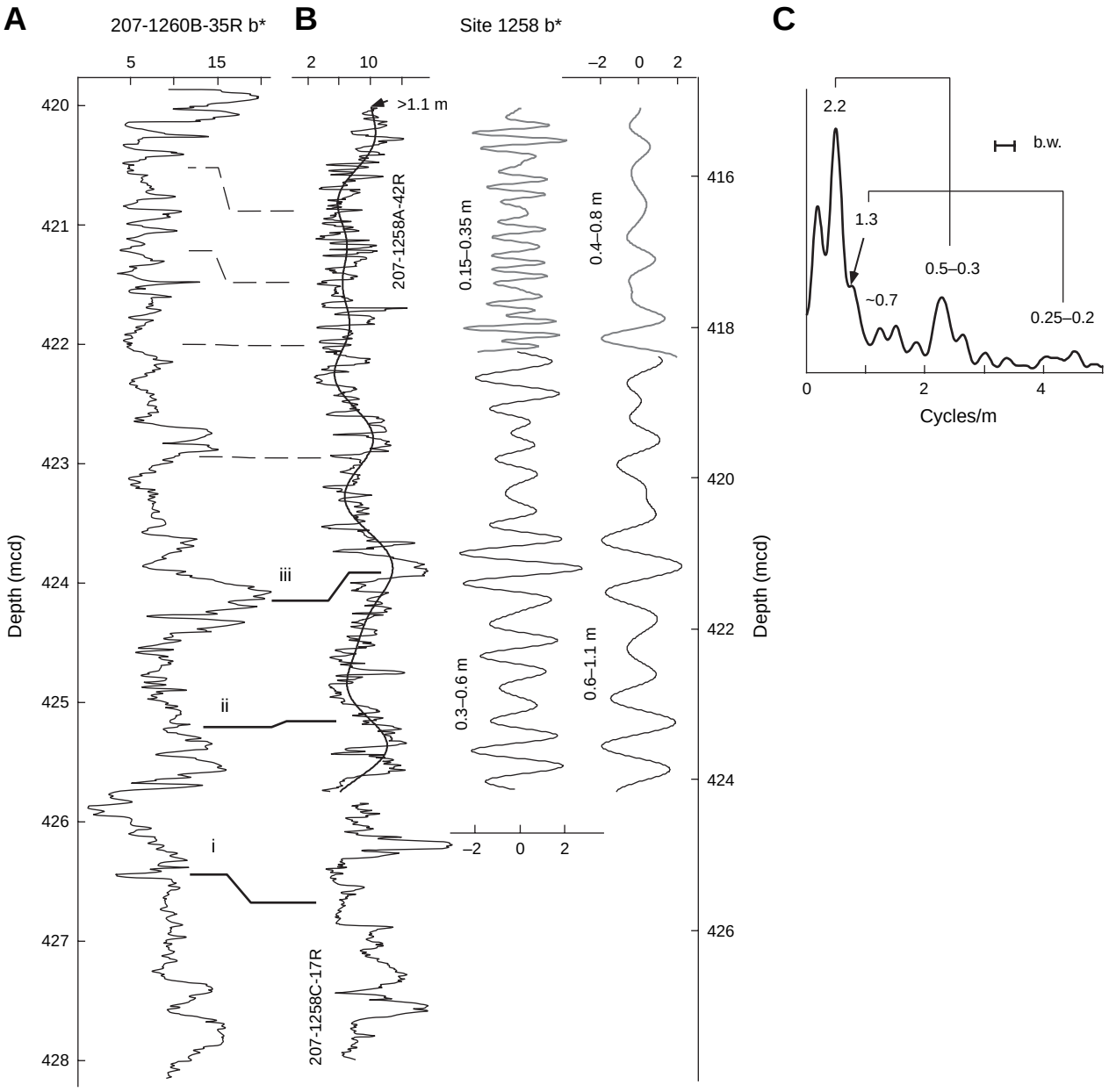

Figure F8. Correlation of $\delta^{13}C$ stratigraphy and sediment color at Site 1258 (Erbacher et al., 2005, and this paper) and Well S75 in the Tarfaya Basin (Kuhnt et al., 2005). Corresponding cycles are marked with letters. Note that the end of the excursion plateau at Site 1258 is here put at the first decrease in $\delta^{13}C$ values and not at the top of the following short excursion as in Erbacher et al. (2005). For further discussion, see text.

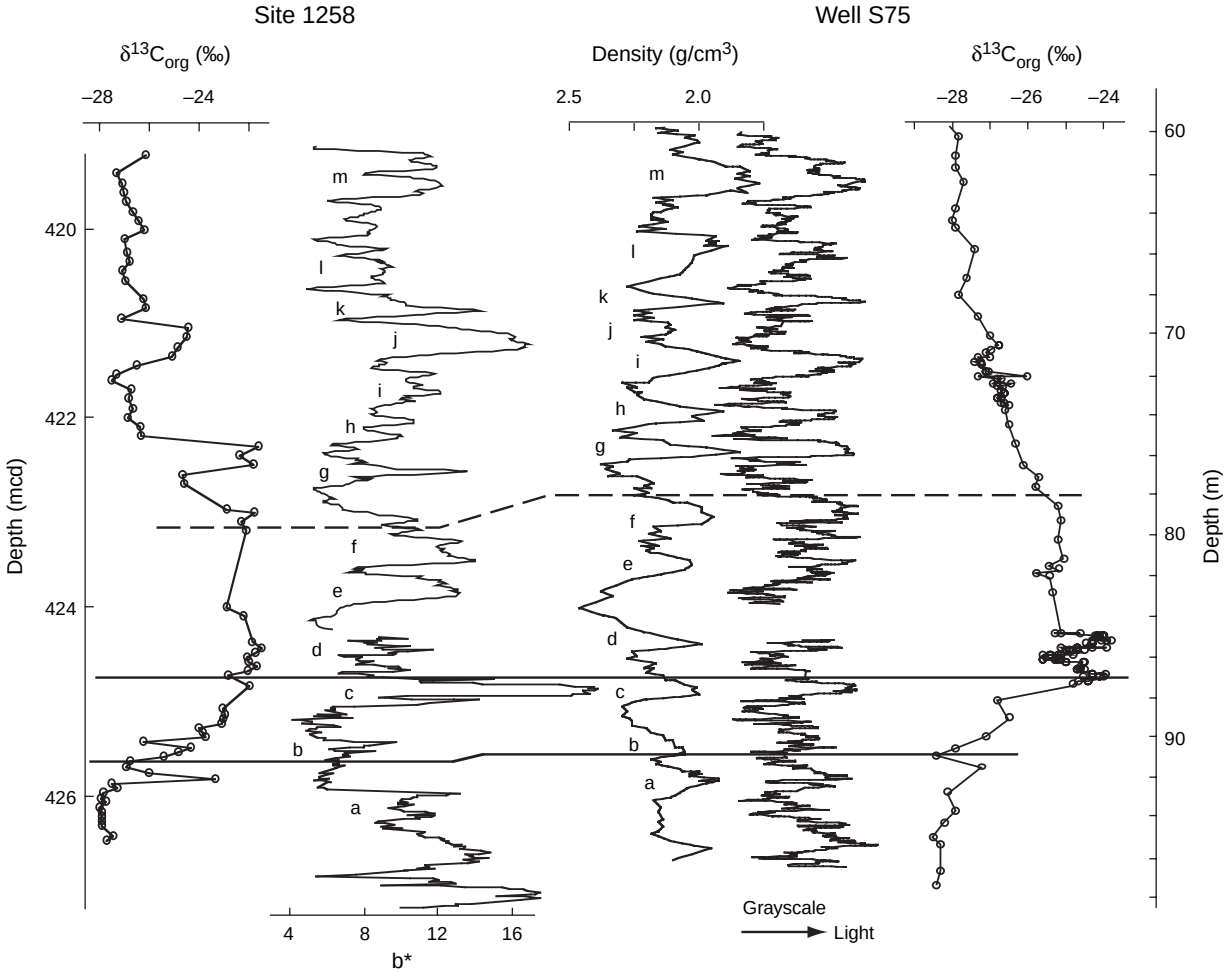

Plate P1. Transmitted light microscope (TLM) photographs (unless stated otherwise). **1.** Shipboard Geoscan II image showing laminated pelagic carbonate-rich interval (interval 207-1257B-21R-2, 26–46 cm; 195.06 mbsf; Turonian). Double arrow indicates position of thin section shown in 2 and 3. **2, 3.** Sample 207-1257B-21R-2, 33–36 cm (195.13 mbsf; Turonian); (2) micritic white laminae and dispersed planktonic foraminifers of variable size; (3) rare large fecal pellet (arrow). **4.** SEM photograph parallel to bedding plane of thin white lamina within predominantly dark colored sediment interval, showing nannofossils concentrated in fecal pellet (Sample 207-1261B-7R-2, 51.5–67 cm; 579.99 mbsf; Coniacian/Santonian). **5.** Shipboard Geoscan II image showing laminated planktonic foraminiferal packstone (interval 207-1259A-59R-4, 100–120 cm; 544.83 mbsf; Turonian). Double arrow indicates position of thin section shown in 6. **6.** Enlargement of 5 showing variation in concentrations of planktonic foraminifers (Sample 207-1259A-59R-4, 110–113 cm; 544.93 mbsf; Turonian). **7.** Example of small fecal pellets and organic matter in organic-rich sediment (Sample 207-1258B-45R-4, 114–117 cm; 401.90 mbsf; OAE2). **8.** BSE image of laminated sediment showing potentially seasonal alternation between irregular laminae with planktonic foraminifers separated by thin clay-rich laminae (white arrows) (Sample 207-1259B-23R-3, 114–115.5 cm; 538.14 mbsf; Turonian).

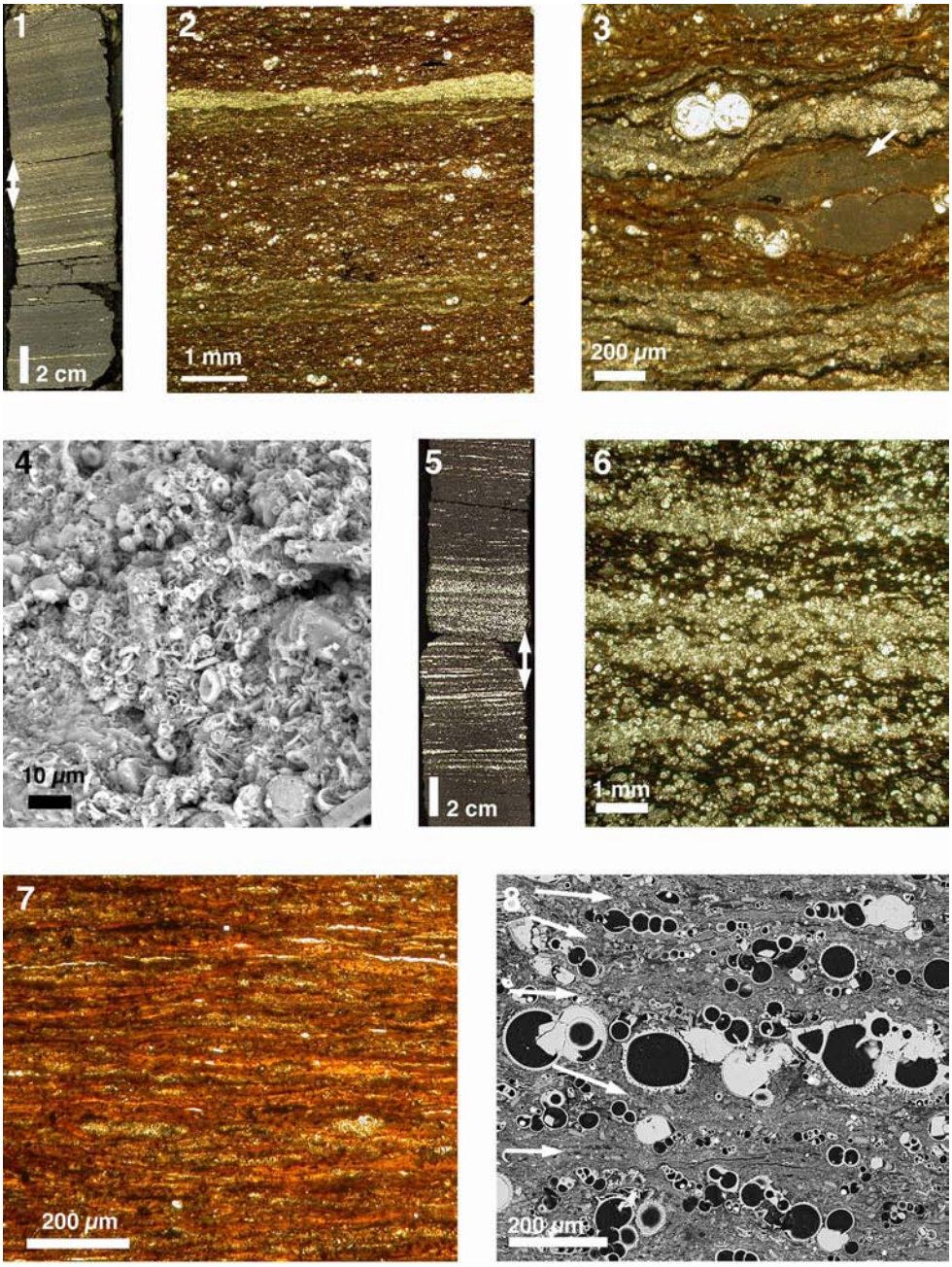

Plate P2. Transmitted light microscope (TLM) photographs. **1.** Detail of a 1-cm-thick planktonic foraminifer packstone, probably a turbidite, within a pelagic organic-rich interval. Note abundant fish debris (Sample 207-1258A-46R-2, 19–20 cm; 424.85 mbsf; Cenomanian). **2.** Gradual transition between foraminiferal wackestone and packstone laminae (Sample 207-1260B-37R-5, 108–111 cm; 441.58 mbsf; Cenomanian). **3.** Planktonic foraminifers clustered within fecal pellets (Sample 207-1260B-34R-2, 115–118 cm; 408.35 mbsf; Turonian). **4.** Coarsely crystalline sparite growing in a pelagic planktonic foraminiferal wackestone (Sample 207-1258A-48R-2, 92–95 cm; 435.21 mbsf; Cenomanian). **5.** Abundant zeolites (arrows) within laminated organic-rich sediment (Sample 207-1258B-45R-4, 114–117 cm; 401.90 mbsf; OAE2). **6.** Calcisphere packstone (Sample 207-1257B-25R-2, 32–35 cm; 214.42 mbsf; Cenomanian).

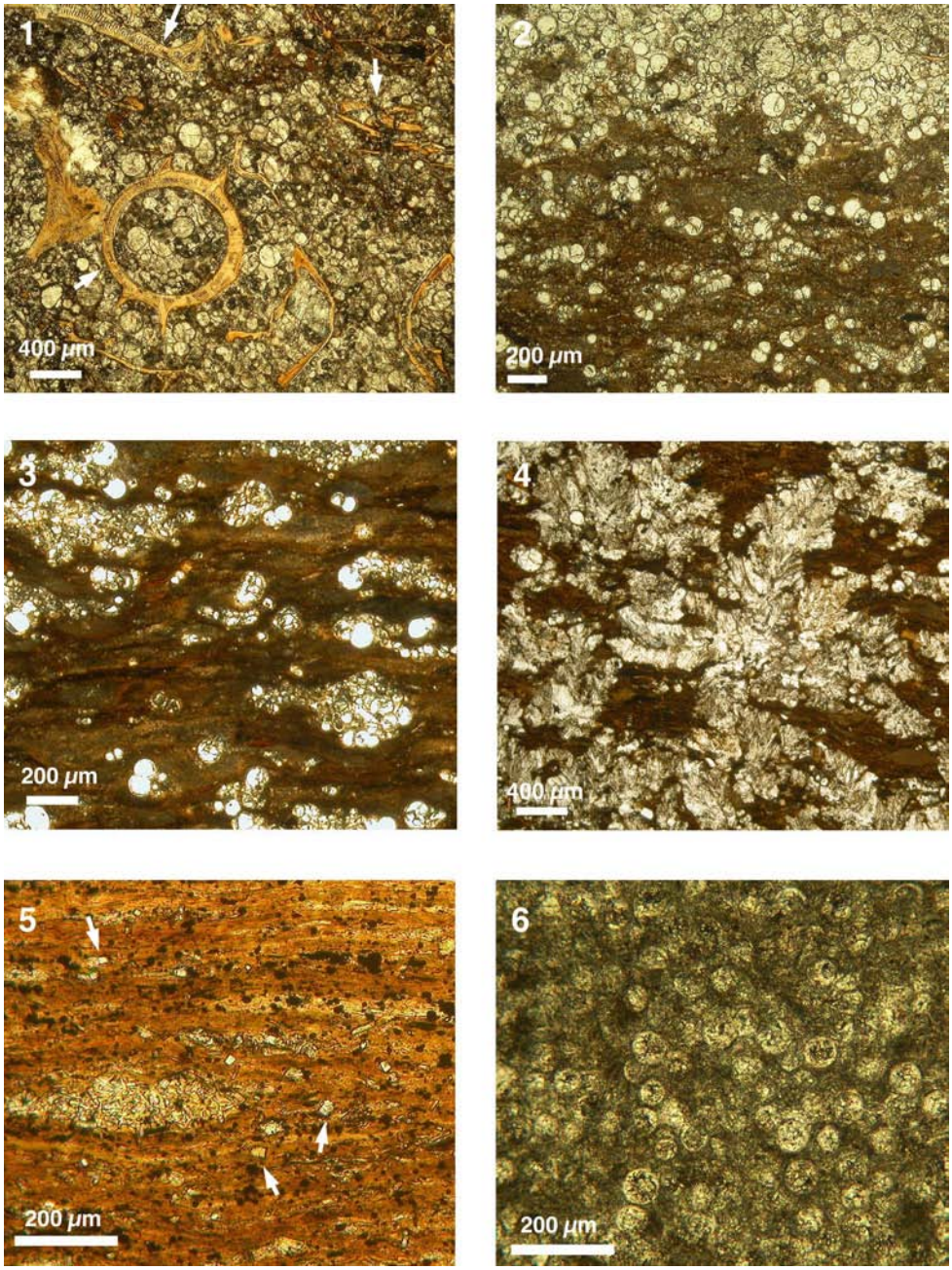

Plate P3. Samples from the OAE2 interval in the Tarfaya Basin quarry (see Fig. F1, p. 21) (transmitted light microscope [TLM] photographs unless stated otherwise). **1.** Flatbed scan of sediment slab from organic-rich level. Note white calcareous nodule and bending of laminae around it (Sample 11A4). **2, 5.** Details from 1 (Sample 11B-1A1); (2) lateral equivalent of 1, showing organic-rich sediment with abundant large flattened fecal pellets (P) and sparse planktonic foraminifers (arrows); (5) limestone nodule in 1. Note that lack of compaction of fecal pellets is indicative for very early diagenetic cementation. **3, 4.** Sample 11A2; (3) BSE image of sediment similar to 2. Note speckled texture in large fecal pellets (E), which is indicative for *Eprolithus floralis* floras as shown in 4; (4) SEM photograph parallel to bedding plane of fecal pellet with near-monospecific *Eprolithus floralis* nannoflora. **6.** Flatbed scan of sediment slab from carbonate-rich level. Note absence of well-defined laminations (Sample 5D/E). **7.** Detail of carbonate-rich sediment as in 6 with sparse planktonic foraminifers (F) and calcified radiolarians (R) (Sample 5E-2B). **8.** Organic-rich sediment showing rare occurrence of lamina with large planktonic foraminifers (F) with filaments (arrows) and fecal pellets (P) (Sample 11B-2B).